JCB Journal of Cell Biology

ARTICLE

A cellular complex of BACE1 and γ-secretase sequentially generates Aβ from its full-length precursor

Lei Liu[1], Li Ding[1], Matteo Rovere[1], Michael S. Wolfe[2], and Dennis J. Selkoe[1]

Intramembrane proteolysis of transmembrane substrates by the presenilin–γ-secretase complex is preceded and regulated by shedding of the substrate's ectodomain by α- or β-secretase. We asked whether β- and γ-secretases interact to mediate efficient sequential processing of APP, generating the amyloid β (Aβ) peptides that initiate Alzheimer's disease. We describe a hitherto unrecognized multiprotease complex containing active β- and γ-secretases. BACE1 coimmunoprecipitated and cofractionated with γ-secretase in cultured cells and in mouse and human brain. An endogenous high molecular weight (HMW) complex (∼5 MD) containing β- and γ-secretases and holo-APP was catalytically active in vitro and generated a full array of Aβ peptides, with physiological Aβ42/40 ratios. The isolated complex responded properly to γ-secretase modulators. Alzheimer's-causing mutations in presenilin altered the Aβ42/40 peptide ratio generated by the HMW β/γ-secretase complex indistinguishably from that observed in whole cells. Thus, Aβ is generated from holo-APP by a BACE1–γ-secretase complex that provides sequential, efficient RIP processing of full-length substrates to final products.

Introduction

The salutary convergence of fundamental biology and the study of human disease is exemplified by the discovery of regulated intramembrane proteolysis (RIP) in the period leading up to 2000. Knowledge of this previously unrecognized biochemical process emerged simultaneously from the study of cholesterol biosynthesis and the amyloidosis of Alzheimer's disease (Brown et al., 2000). Site 2 protease became the first known intramembrane metalloprotease when it was found to hydrolyze its principal substrate (sterol regulatory element binding protein) within the lipid bilayer (Rawson et al., 1997). In an analogous fashion, presenilin (PS) was identified as the first intramembrane aspartyl protease based on its regulated cleavage of the amyloid β (Aβ) precursor protein (APP) to generate Aβ proteins (Wolfe et al., 1999). "Regulated" in the term RIP refers to the requirement for the intramembrane scission to be preceded by shedding of the substrate's ectodomain, by site-1-protease in the case of S2P and by an α-secretase (e.g., ADAM10) in the case of APP.

PS is the catalytic subunit of the γ-secretase complex (Wolfe et al., 1999), which also contains nicastrin (NCT), Aph-1, and Pen-2 (Edbauer et al., 2003; Kimberly et al., 2003; Takasugi et al., 2003). It has been found to have >100 single-transmembrane substrates, including Notch, Jagged, and ErbB4 (Haapasalo and Kovacs, 2011). As such, PS mediates a remarkably diverse array of signaling functions necessary for life in metazoans from worm to man. Besides having its ectodomain shed by α-secretases such as ADAM10 or ADAM17, APP can instead undergo shedding ∼16 residues N-terminal to the α-secretase cut site by the β-secretases. The latter comprise membrane-anchored aspartyl proteases designated Aβ cleaving enzyme (BACE) 1 and BACE2. BACE1 is highly expressed in neurons and is the protease making the first cut in holo-APP to shed its large N-terminal ectodomain (sAPP-β), followed by cleavage of the membrane-retained C-terminal APP fragment (CTFβ or C99) by γ-secretase to release the Aβ peptides (Vassar et al., 2014). These N- and C-terminally heterogeneous peptides are secreted by neurons and many other cells throughout life (Haass et al., 1992). With age, a portion of the longer, more hydrophobic Aβ peptides (Aβ42, Aβ43) tends to aggregate into cytotoxic oligomers and amyloid fibrils, which form the hallmark neuritic (amyloid) plaques of Alzheimer's disease (Selkoe and Hardy, 2016).

In the last few years, there has been substantial progress in deciphering the 20-transmembrane domain (TMD) structure of the PS–γ-secretase complex (e.g., Sato et al., 2006; Bai et al., 2015a,b; Sun et al., 2015). Complementary to this structural

[1]Ann Romney Center for Neurologic Diseases, Department of Neurology, Brigham and Women's Hospital, Harvard Medical School, Boston, MA; [2]University of Kansas School of Pharmacy, Department of Medical Chemistry, Lawrence, KS.

Correspondence to Dennis J. Selkoe: dselkoe@bwh.harvard.edu.

https://doi.org/10.1083/jcb.201806205

advance, biochemical studies have illuminated how APP (and presumably all other γ-substrates) undergoes stepwise ("processive") proteolysis at the ε, ζ, and γ cleavage sites, that is, every three to four residues within the transmembrane helix (Bolduc et al., 2016b). In addition, the role of NCT in sterically preventing entry of large, full-length substrates into the PS active site before their ectodomain shedding has been identified (Bolduc et al., 2016a). On the other hand, we still know very little about the cell biological mechanism of the two-step processing that defines RIP. It has been assumed that the post-sheddase CTFs are trafficked to a membrane site where γ-secretase is active, but how such presumptive movement in the membrane occurs so that the CTF correctly finds and enters first the docking and then the active site of γ-secretase remains a mystery. It is this central feature of RIP that we probe in the current study.

We based our experimental approach on our recent discovery that substrate processing by α- and γ-secretases can occur in a large, multiprotease fraction that allows for sequential cleavage of substrates within a high molecular weight (MW [HMW]) complex stabilized by members of the tetraspanin web (Chen et al., 2015). This unexpected finding of coordinated α/γ processing raised the question of whether a similar mechanism exists for the β- and γ-secretase cleavages that generate Aβ from APP and create analogous protein fragments from many other β/γ substrates. Here, we used coimmunoprecipitation (coIP), nondenaturing fast protein liquid chromatography (FPLC), and novel Aβ ELISAs to identify an endogenous HMW complex (∼5 MD) in normal mouse and human brain that contains mature, proteolytically active β- and γ-secretases. FPLC fractions containing this native complex generated a range of physiological Aβ peptides from endogenous holo-APP upon incubation at 37°C, which we refer to as de novo Aβ generation. Importantly, the majority of cellular BACE1 protein and the APP-CTFβ fragment was found in low MW (LMW) FPLC fractions that did not contribute to Aβ generation; Aβ peptides could not be generated from these LMW fractions despite their abundant BACE1. Instead, we found that the active β/γ complex could be pulled down from HMW FPLC fractions by antibodies to PS, NCT, or the APP holo-protein (holo-APP); the APP pull-down, in particular, generated readily detectable amounts of multiple Aβ peptides from holo-APP, with an Aβ42/40 ratio of ∼0.1 that perfectly matches the physiological ratio in human biological fluids. Two classes of clinically relevant γ-secretase modulators (GSMs; E2012 and JNJ-40418677) decreased new Aβ42 generation by the complex in vitro and shifted it to an increased Aβ37 generation. Familial AD mutations in PS1 caused the β/γ complex to generate pathologically elevated Aβ42/40 ratios like those found in patients. We conclude that Aβ generation in human brain occurs from an endogenous BACE1–γ-secretase complex that also contains docked holo-APP, which undergoes sequential β- and γ-secretase cleavages to generate diverse Aβ peptides throughout life.

Results

BACE1 physically associates with the γ-secretase complex in mouse brain lysates

We recently reported preliminary evidence that BACE1 can be coimmunoprecipitated with γ-secretase in unfractionated normal mouse brain (see Fig. 10, A and B, in Chen et al., 2015). We have now conducted several more controls to confirm the specificity of this apparent β/γ association in microsomes prepared from 1% CHAPSO homogenates of WT mouse brain. Antibodies to BACE1 consistently coimmunoprecipitated mature PS1 and NCT, whereas antibodies against three other type I transmembrane proteins, ITGα1, ITGα2, and ITGβ1, yielded no such association (Fig. 1 A), even though the latter antibodies coimmunoprecipitated their respective target proteins successfully (Fig. S1 D). Because the critical micelle concentration of CHAPSO is ∼0.5%, we proceeded to confirm the β/γ-secretase association at submicellar concentrations (i.e., in 0.25% CHAPSO lysates of WT mouse brain) and obtained the same results using two distinct BACE1 antibodies, while ITGα1 IP was again negative (Fig. S1 A). To further test the specificity of our BACE1–γ-secretase pull-down, we performed an additional wash step of the BACE1 IP in 2% NP-40, which is known to disrupt any coprecipitated γ-secretase complex (Chen et al., 2010). This removed the PS1-CTF and PS1-NTF from the BACE1 immunoprecipitate (Fig. S1 B, lanes 3 and 5). Analysis of the protein complexes using 2D Blue Native (BN)/SDS gel electrophoresis of mouse brain microsomes solubilized in 1% CHAPSO revealed that just the HMW portion of BACE1 (>500 kD) comigrated with the mature γ-secretase subunits PS1-NTF and PS1-CTF in the native first dimension (Fig. 1 B). In contrast, the distribution of mature ADAM10 (A10) largely overlapped with the mature γ-secretase components (PS1-NTF, PS1-CTF, and NCT), as previously reported (Chen et al., 2015). Next, we applied the same 2D BN/SDS system but using 0.5% n-dodecyl-B-D-maltoside (DDM) detergent instead of CHAPSO to prepare the brain lysates. As expected from prior studies of γ-secretase with DDM (Fraering et al., 2004a), the integrity of the β/γ complex was disrupted and shifted to smaller MW (<500 kD) positions (compare Fig. S1 C with Fig. 1 B). Collectively, these data suggest an interaction between BACE1 and the γ-secretase complex in normal brain tissue and the existence of a macromolecular complex that remains intact in 1% CHAPSO but not in stronger detergents.

BACE1 and γ-secretase coexist in a HMW complex

Next, we prepared microsomes from WT mouse brain in 1% CHAPSO buffer and size fractionated their proteins on a Superose 6 Increase size exclusive chromatography (SEC) column using an FPLC system. (CHAPSO is among the few detergents that allow the five obligatory protein subunits of γ-secretase [PS1-NTF, PS1-CTF, NCT, Aph-1, and Pen-2] to remain together in a functional complex.) Each of the 24 FPLC fractions was lyophilized and probed by immunoblotting (Fig. 2 A). Mature A10, Meprin-β, and a portion of BACE1 cofractionated with the mature γ-secretase complex, represented by mature NCT, PS1-CTF, PS1-NTF, and Aph-1 (the PS2-CTF was also present in this HMW region, as expected for this endogenous PS1 homologue). These HMW FPLC fractions are estimated to be >5,000 kD (5 MD; see Fig. S3 A for column sizing standards). Immature NCT and immature PS1 (i.e., PS1 holoprotein) eluted in LMW fractions estimated to be <160 kD (Fig. 2 A). In contrast to α-secretase (mature A10), there was an appreciable amount of β-secretase (BACE1) visible in the LMW column fractions by Western blot (WB), which is consistent with

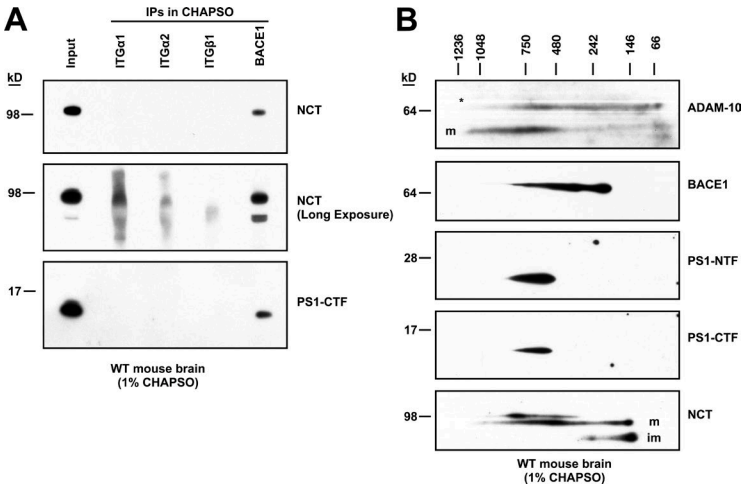

Figure 1. **The β-secretase BACE1 interacts with γ-secretase at endogenous levels in WT mouse brain microsomal lysate. (A)** 1% CHAPSO-solubilized lysates of WT mouse brain microsomes were immunoprecipitated for BACE1 or ITGα1, ITGα2, and ITGβ1 as controls. IPs were blotted to probe for coIP of the γ-components NCT and PS1-NTF. **(B)** 1% CHAPSO-solubilized lysates of WT mouse brain microsomes were loaded onto BN-PAGE followed by second-dimension SDS-PAGE and blotted with antibodies to the indicated proteins. *, nonspecific signal; m and im, mature and immature forms.

our 2D BN/SDS blots (Fig. 1 B). We next analyzed concentrated pools of the HMW fractions (#6–9) versus the LMW fractions (#21–24) by 2D electrophoresis. In the HMW pool, 2D BN/SDS revealed that PS1-CTF and BACE1 comigrated at >1,000 kD, while in the LMW pool, BACE1 migrated at ∼200 kD in the absence of mature PS1 NTF/CTF (Fig. S2 A). We immunoprecipitated BACE1 from both the HMW and LMW FPLC pools and found that BACE1 coimmunoprecipitated with mature PS1-CTF and mature NCT only from the HMW pool, although the LMW pool has abundant BACE1 (Fig. 2 B). We blotted analogous fractions from another FPLC run with an APP antibody that recognizes both FL-APP (holoprotein) and its CTFα fragment that arises from α-secretase cleavage (Fig. 2 C). FL-APP cofractionated in substantial part with the mature γ-secretase complex, whereas the CTFα product accumulated mostly in the LMW fractions (Fig. 2, compare C with A). Also, we observed a ∼30-kD APP-immunoreactive band specifically in LMW fractions #21–24 (Fig. 2 C, bottom panel), which we found to be consistent with the recently reported APP-CTFη (eta cleavage product; Willem et al., 2015) by using an antibody (1G6) to the "pre-β" region of APP just N-terminal to the BACE1 cleavage site (see Fig. S2 D). APP-CTFη was reported to be a product of proteolysis of FL-APP by MT5-MMP (the η-secretase; Willem et al., 2015). We probed the FPLC fractions with an MT5-MMP antibody and saw bands of the correct MW in the LMW fractions (#21 and #22; Fig. 2 A). This η-secretase thus served as a negative-control sheddase that does not form natural complexes with γ-secretase, consistent with the previous work detecting Aη-α and Aη-β APP fragments but no Aη-γ fragment, which would require γ-secretase to generate (Willem et al., 2015). To extend our findings, we probed for two more known β/γ substrates in our FPLC fractions, LRP-1 and APLP-1, and these had similar size distributions as FL-APP (Fig. S2 B).

In light of this apparent evidence for a potentially common phenomenon of a sheddase (A10 or BACE1) complexing with an intramembrane protease (PS–γ-secretase), we proceeded to test the FPLC migration of three other intramembrane proteases: SPP, SPPL2b, and RHBDL2 (Fig. S2 B). Endogenous SPPL2b eluted in the HMW fractions with the γ-secretase complex, whereas endogenous SPP and RHBDL2 each eluted in the LMW fractions (Fig. S2 B). In this regard, SPPL2b is reported to cleave its Bri-2 substrate intramembranously after Bri-2's ectodomain is shed by A10 (Martin et al., 2008). 2D BN/SDS-PAGE results for SPP and RHBDL2 confirmed the FPLC results (Fig. S2 C). Collectively, the findings so far suggest the existence of an endogenous HMW complex containing BACE1 and PS–γ-secretase.

The β/γ-secretase complex is proteolytically active

Using a well-characterized fluorogenic peptide substrate to assay β-secretase activity (Ermolieff et al., 2000), we observed much higher BACE1 cleavage activity in the LMW than in the HMW FPLC fractions (Fig. 2 D), closely paralleling the distribution of the protease across the fractions (Fig. 2 A). We then asked whether the immunoprecipitable β/γ complexes found selectively in the HMW fractions (Fig. 2 B) contain BACE1 proteolytic activity. Using antibodies to NCT (or TfR as a negative control) to pull down the β/γ complex from 1% CHAPSO-solubilized microsomes of WT mouse brain, the coimmunoprecipitated complex was eluted and then incubated at 37°C for 2 h with the fluorogenic peptide substrate. AZD3293 or Inhibitor IV was used to specifically confirm the BACE1 reaction. Anti-NCT (but not anti-TfR) precipitated protein complexes from the microsomes having β-secretase activity, which could be inhibited by pretreating the samples with either BACE1 inhibitor, showing the specificity of this assay (Fig. 2 E). We then used the same approach to try to pull down active β/γ complexes from the HMW and LMW pools of FPLC fractions. Consistent with the IP-WBs of these two pools (Fig. 2 B), the NCT-IP from the HMW pool yielded β-secretase activity while that from the LMW pool (which lacks NCT) did not, as expected (Fig. 2 F). After calibrating these activity signals using recombinant human BACE1 as a standard (Fig. S2 E, left graph), the BACE1 activities of the β/γ complexes from both the unfractionated mouse brain lysate (Fig. S2 E, middle graph) and from the HMW pool (Fig. S2 E, right graph) were significantly greater than that of the control samples (the TfR IP or the NCT IP pretreated with a BACE1 inhibitor; Fig. S2 E). Together, our findings demonstrate that an endogenous HMW β/γ-secretase complex has BACE1 catalytic activity. Next, we asked whether this novel secretase complex could mediate sequential APP substrate cleavages to release the final products (Aβ peptides) in cultured cells.

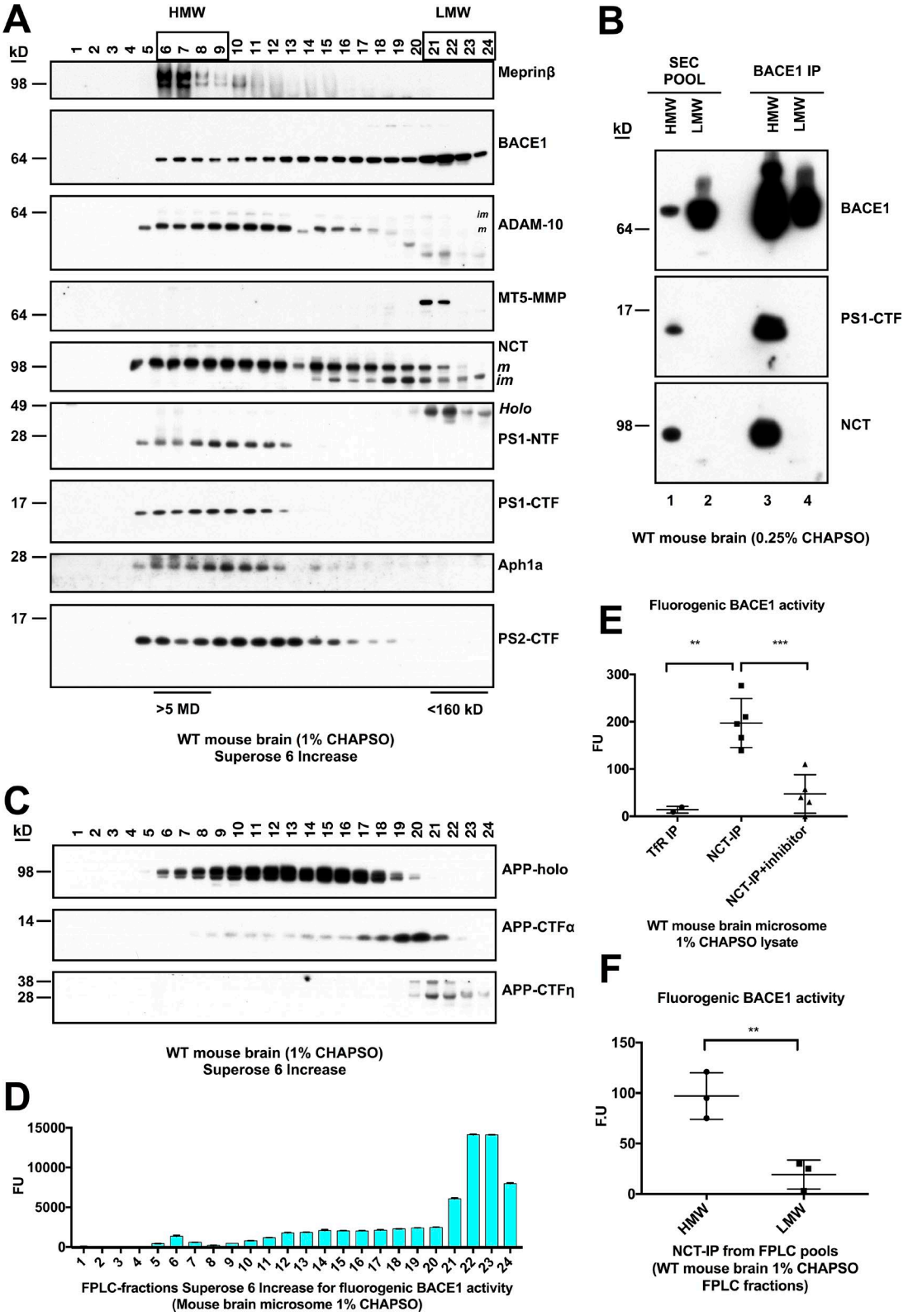

Figure 2. **BACE1 exists with γ-secretase in an HMW complex isolated from mouse brain by FPLC and has proteolytic activity. (A)** 1% CHAPSO-solubilized WT mouse brain microsomes were fractionated on a Superose 6 Increase SEC column by FPLC and blotted with antibodies to the indicated proteins. **(B)** FPLC fractions were pooled into HMW (6–9) or LMW (21–24) fractions and immunoprecipitated for BACE1 and then blotted with antibodies to the indicated proteins. Note that the amount of BACE1 that was immunoprecipitated varies and may not necessarily reflect the amount in the input. **(C)** FPLC fractions were blotted with certain antibodies to APP (top two panels, C7; bottom panel, 1G6). **(D)** FPLC fractions were incubated with a fluorogenic BACE1 peptide substrate. After incubation for 2 h at 37°C, fluorescence was read as BACE1 activity (n = 3; error bars are SD). **(E)** 0.25% CHAPSO-solubilized WT mouse brain microsomes were immunoprecipitated for γ-secretase (anti-NCT) in the absence or presence of two different β-secretase inhibitors (AZD3293 and inhibitor IV,

The HMW β/γ-secretase complex is responsible for the majority of Aβ production

We showed above that in native FPLC fractions of WT mouse brain homogenates, the major portions of both BACE1 protein and BACE1 peptide cleavage activity are found in the LMW pool (Fig. 2, A and D). We next used FPLC fractions of HEK293 cells stably expressing human swAPP to probe for the functional contribution of the HMW β/γ-secretase complexes to Aβ production. We examined FPLC fractions by immunoblots (Fig. 3 A). Of note, the size distribution of the γ-secretase complex across the FPLC fractions is somewhat different in these human cells (Fig. 3 A, top four panels) than in mouse brain (Fig. 2 A, bottom five panels); this different distribution is also apparent on our 2D BN/SDS-PAGE blots for PS1-NTF in 1% CHAPSO microsomes (compare size migration of PS1-NTF in Figs. 3 B and 1 B), consistent with a prior report (Gu et al., 2004). When we examined FPLC fractions from HEK293 cells by immunoblots (Fig. 3 A) and ELISA (Fig. S3 C), we found that the unprocessed APP-CTFβ is present in both the HMW and LMW fractions. By performing immunoblotting and the BACE1 ELISA on the same FPLC fractions, we observed a closely similar distribution of the BACE1 protein across the fractions of the HEK293 cells (Figs. 3 A and S3 B) as we had observed by WB in mouse brain (Fig. 2 A).

Next, we designed a novel experimental paradigm to exam the enzymatic activity and related physiological properties of the HMW β/γ-secretase complexes. As diagrammed in Fig. S3 D, we used 1% CHAPSO lysates of the HEK293/swAPP cell microsomes as the input material. After fractionation by FPLC (Superose 6 Increase) in 0.25% CHAPSO, we incubated the resultant FPLC fractions at 37°C with nutation for 12 h (Fig. S3 D, left). We sought to detect substrate (holo-APP) within the HMW β/γ-secretase complexes to search for its sequential cleavages into final products (Aβ peptides), an in vitro process we term de novo Aβ generation. After the 37°C incubation, each sample was lyophilized, and the powder was reconstituted in 0.05% Triton X-100. Aβx-40 and Aβx-42 were measured by ELISA and their ratio was established (Fig. 3 C). Most newly generated Aβx-40 and Aβx-42 occurred in the HMW fractions, and the 42/40 ratio was 0.1–0.2 in the active fractions (#5–7) that generated most Aβ; this is the physiological ratio found in normal human biological fluids. These data suggested that only the HMW complex (>5 MD) containing both BACE1 and γ-secretase has physiological Aβ-generating activity. Next, we added 5 µM L685,458 (a potent transition-state analog [TSA] inhibitor of γ-secretase which binds at the active site) into the FPLC fractions before the 37°C incubation (DMSO vehicle was the control). Surprisingly, L685,458 failed to inhibit the de novo Aβ generation (Fig. 3 D). We speculated that this result could be explained if the holo-APP substrate was already docked into the catalytic site of γ-secretase so that L685,458 could not efficiently bind there and inhibit (addressed below). We next asked whether de novo Aβ generation from the HMW fractions could instead be modulated allosterically by GSMs. We added 10 µM JNJ-40418677, an NSAID-derived GSM, to the FPLC fractions (versus just DMSO) before the 37°C incubation. This compound decreased Aβx-42 and Aβx-40 production and increased Aβx-37 production (Fig. 3 E), indicating that de novo Aβ generation by the HMW complexes can be allosterically modulated by a GSM.

To confirm that the de novo Aβ generation we observed derived from holo-APP, we pretreated intact HEK293-swAPP cells for 24 h with the BACE1 inhibitor AZD3293 (2.5 µM), which prevents APP-CTFβ generation (Fig. 7 D). Then, FPLC fractions of the pretreated cells were used for the de novo Aβ generation reaction. As shown in Fig. 3 F, there were 1.5- to 4-fold increases in Aβx-40 de novo production in FPLC fractions #5–8 despite the prior treatment with the BACE1 inhibitor, which had been washed out during the FPLC. We hypothesized that this increased de novo Aβ generation was derived from holo-APP that had accumulated in the HMW fractions during the AZD3293 pretreatment. To support this interpretation, we blotted for holo-APP in FPLC fractions of cells that had been treated with DMSO or AZD3293 before the de novo Aβ generation (Fig. 3 G). We observed an increase in holo-APP protein in the HMW fractions (#5–9) that generate Aβ, and this was specifically in the mature, N+O-glycosylated APP known to be the preferred substrate for BACE1 cleavage (e.g., Tomita et al., 1998). We quantified the amount of mature APP in fractions #5–10 of cells treated with AZD3293 or just DMSO before the de novo Aβ generation and observed a statistically significant increase of mature APP in fractions #6–10 after AZD3293 treatment (Fig. S3 E). There was no significant change of PS1-NTF in the same fractions following the BACE1 inhibition (Fig. 3 G). Collectively, these data provide direct evidence that BACE1 inhibition leads to the accumulation of mature (N+O-glycosylated) holo-APP in HMW fractions, which can subsequently undergo sequential cleavages by the β/γ complex to generate Aβ once the BACE1 inhibitor is washed out.

We further characterized the HMW complex to confirm that Aβ generation from holo-APP represents sequential processing by the β/γ secretase complex. A preparative SEC column, Sephacryl S-300 HR, was used instead of the analytical Superose 6 Increase SEC column to enable bulk preparation of β/γ HMW complexes from HEK293-swAPP microsome lysates. (The performances of Superose 6 Increase and S-300 HR FPLC columns were compared by running MW calibration standards [Figs. S3 A and S4 A, top] and the 1% CHAPSO microsome samples [Figs. S3 A and S4 A, bottom].) We used the first eight HMW fractions after the void volume of the S-300 HR column to probe for de novo Aβ generation at 37°C (Fig. 4 A). Fractions #1–4 collectively generated the vast majority of de novo Aβ (including Aβx-37, Aβx-40, and Aβx-42). We also quantified basal Aβx-40 levels in the FPLC fractions present before the 37°C incubation to assess how much existing Aβ was carried over from the microsome preparations; this comprised only ∼20% of the Aβx-40 amount present after the de

each at 10 µM), or else anti-TfR as a control. β-Secretase activity assays were performed on the eluates extracted from the IP resin. *n* = 5 for the NCT IP, *n* = 2 for the TfR IP; error bars are SD. Unpaired Student's *t* test: **, P < 0.01; ***, P < 0.001. **(F)** Pooled HMW and LMW FPLC fractions from WT mouse brains were immunoprecipitated for γ-secretase (anti-NCT). β-Secretase activity assays were performed on the eluates extracted from the IP resin (unpaired Student's *t* test: **, P < 0.01, *n* = 3; error bars are SD).

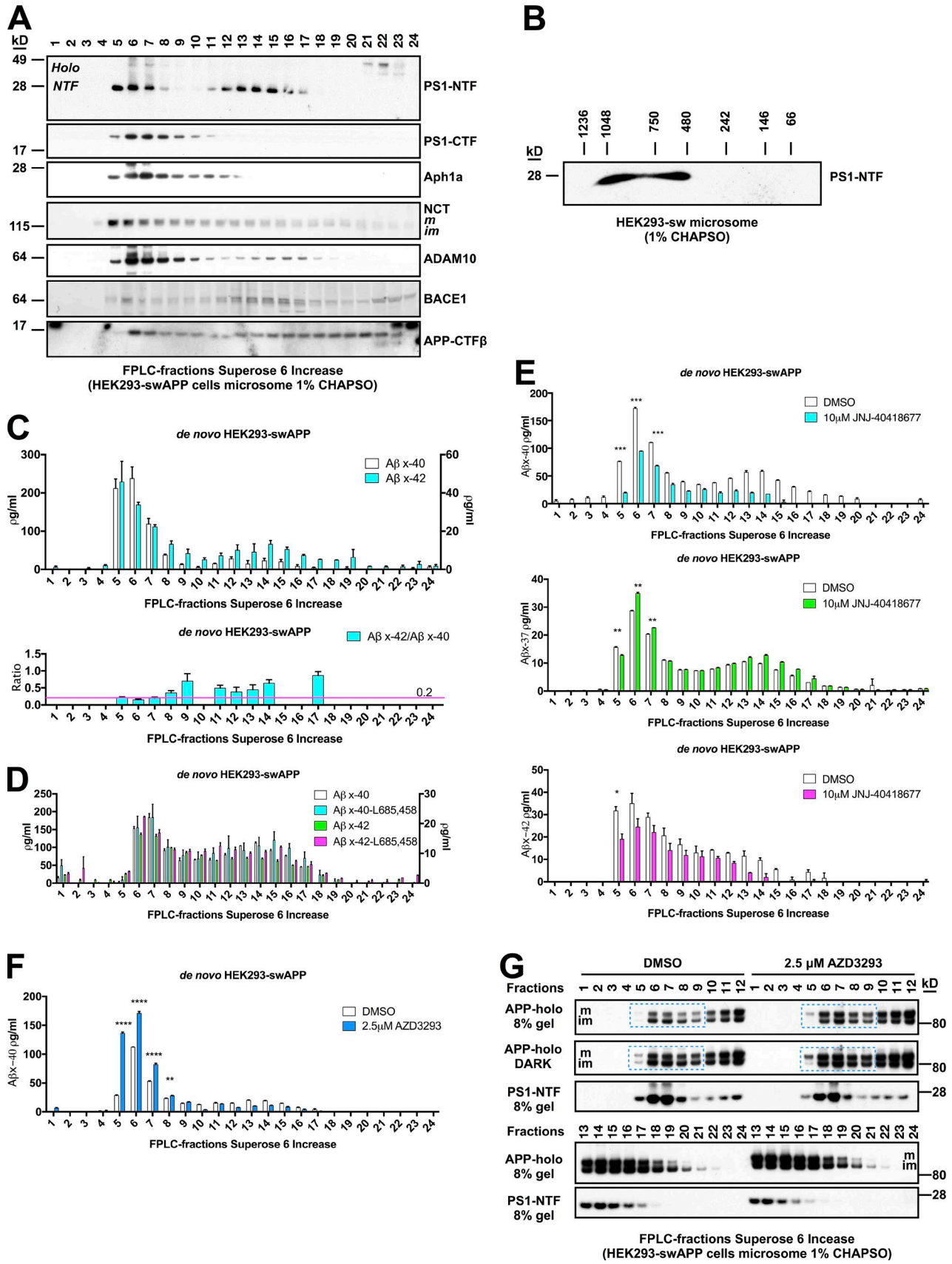

Figure 3. **De novo Aβ generation in HMW FPLC fractions of microsomes from HEK293-swAPP cells. (A)** FPLC fractions (Superose 6 Increase column) of 1% CHAPSO-solubilized microsomes of HEK293/swAPP cells were blotted with antibodies to the indicated proteins. **(B)** Unfractionated microsomes were loaded onto 2D BN/SDS-PAGE and blotted for PS1-NTF. **(C)** FPLC fractions were incubated at 37°C for 12 h. Aβx-40 and x-42 de novo generation was quantified by

novo incubation (Fig. 4 A, fractions #1 and 2). Protein levels of holo-APP, BACE1, and γ-secretase (NCT, PS1-NTF, and PS1-CTF) across the eight FPLC fractions were measured by immunoblotting (Fig. S4 C). We next tested two types of GSMs, E2012 (IC50 for Aβx-42 = 53 nM) and JNJ-40418677 (IC50 for Aβx-42 = 190 nM; Jumpertz et al., 2012) to attempt to modulate the de novo Aβ generation by FPLC fraction #1. Pretreatment with either GSM decreased new Aβx-42 generation significantly (Fig. 4 B, top), but JNJ-40418677 performed more efficiently and in a dose-dependent manner to decrease Aβx-40 (Fig. 4 B, middle) and increase Aβx-37 generation (Fig. 4 B, bottom), compared with E2012.

Importantly, we next performed coIPs on FPLC fractions #2–5 to directly immunoisolate β/γ secretase complexes, using antibodies to either the N terminus of holo-APP (22C11), the PS1-NTF (Poly18111), the C terminus of NCT (N1660), or the C terminus of BACE1 (cocktail of Poly8401 and 8402; Fig. S4 B). The IP beads were washed three times and incubated at 37°C in 0.25% CHAPSO reaction buffer for 12 h. De novo Aβ generation was measured in the 0.25% CHAPSO reaction supernatant (Fig. 4 C). Among the HMW complexes immunoprecipitated from the major Aβ-generating FPLC fractions #2–4, generation of both de novo Aβx-40 and Aβx-42 was detectable in the IP of holo-APP, while just Aβx-40 generation was sufficient to be detectable in the IPs of NCT, PS1, and BACE1. Immunoblots of the respective immunoprecipitated complexes confirmed the pull-down of PS-1 and NCT from fractions #2–4 (Fig. S4 D). Of note, the HMW complex pulled down by the holo-APP IP yielded an Aβx-40/42 ratio (~0.1) that was physiological. These key findings confirm sequential cleavage of holo-APP by an immunoisolated HMW secretase complex containing both β and γ proteolytic activities.

Collectively, the above results show that a substrate (in our case holo-APP) that localizes in the >5 MD HMW complex can be coimmunoprecipitated and then processed by endogenous β- and γ-secretases into its final product (in our case physiological Aβ peptides). Thus, a population of HMW β/γ-secretase complexes in cells mediates the serial cleavage of the distal ectodomain and the intramembrane domain of single-transmembrane substrates in a coordinated manner.

Similar HMW β/γ-secretase complexes are observed in human brain

We asked whether the de novo generation of Aβ from the >5 MD HMW complex containing the β- and γ-secretases could be observed in human brain tissue. Fig. 5 A shows our modified protocol to prepare such HMW complexes from human brain. We confirmed the presence of ADAM-10, BACE1, PS-1 (NTF and CTF), Aph-1, FL-APP, and NCT in the FPLC fractions by immunoblot. The distribution of the components of the γ-complex was similar to that of HEK293 cells (Fig. 5 B). We also detected BACE1 proteolytic activity by incubating the BACE1 fluorogenic substrate in the individual FPLC fractions of human brain, revealing a similar distribution pattern to that of mouse brain (Fig. 5 C). Moreover, using microsome lysates from a fresh human brain, we observed similar de novo Aβ generation from the >5 MD HMW complex, particularly in FPLC fractions #5–7 (Fig. 5 D). Next, we added three γ-secretase inhibitors (2 μM Compound E, 5 μM DAPT, or 5 μM L685,458) to the FPLC fractions of human fresh brain microsomes (Fig. 5 E). Each could inhibit only a small portion of de novo Aβ generation, again suggesting that the HMW β/γ-secretase complex is mature and docked with substrate in the catalytic site: both a TSA and a non-TSA γ-inhibitor could not compete with the docked substrate, as the TSA is known to occupy the catalytic site and the non-TSA is known to allosterically change the substrate's binding (Kornilova et al., 2005; Li et al., 2014). Next, we used the GSM JNJ-40418677 (10 μM) on FPLC fractions from a frozen human brain and observed a significantly increased Aβx-37 de novo generation versus vehicle alone (Fig. 5 F). Together, these findings suggest the existence of proteolytically active HMW β/γ-secretase complexes that produce a majority of cellular Aβ in both a human cell line and human brain tissue.

Next, we investigated the nature of the physical association between β and γ secretase in the HMW complexes. As suggested in Fig. 2 A, we reasoned that MT5-MMP could serve as a negative control sheddase which does not form a complex with γ-secretase since it does not generate APP fragments that end at the γ-secretase cleavage site (Fig. S2 D). As RIP proteases are intramembrane cleaving enzymes, we suspected the TMD to be a critical functional domain for HMW complex formation. After aligning the TMDs of BACE1 and MT5-MMP (the identified η-secretase; Willem et al., 2015; Baranger et al., 2016), we generated a chimeric BACE1 molecule by swapping in the TMD of MT5-MMP (Fig. S5 A). We also generated a HEK293/swAPP cell line having a knockout (KO) of endogenous BACE1 and documented a >90% decrease in Aβ secretion compared with its parental line (Fig. S5 B). We then tested whether transfection of WT BACE1 or the MT5-BACE1 TMD chimera could rescue Aβ production in the BACE1 KO cells, compared with either empty vector or GFP as the negative control. WT BACE1 and MT5-BACE1 equally restored Aβ production, whereas the negative controls did not (Fig. S5 C). Moreover, both WT BACE1 and MT5-BACE1 equally coimmunoprecipitated PS1-NTF and NCT from 0.25% CHAPSO-solubilized microsomes of BACE1 KO cells expressing these constructs (Fig. S5 D). Thus, a specific TMD sequence is not crucial for the formation of the proteolytically active HMW complex of β- and γ-secretase, as expected.

ELISA from each fraction after concentration; left y-axis, Aβx-40; right y-axis, Aβx-42 (n = 3; mean ± SD). Below: A relative ratio of Aβx-42/x-40 was calculated; the purple line represents 0.2. **(D)** FPLC fractions were incubated at 37°C for 12 h with L685,458 (5 μM) and with DMSO as the control. Aβx-40/x-42 de novo generation was measured by ELISA on each fraction after concentration (n = 2; means ± SD). **(E)** As in D, fractions #1–24 were incubated at 37°C for 12 h with 10 μM JNJ-40418677 or DMSO as the control. Aβx-37/x-40/x-42 de novo generation were measured by ELISA from each fraction (n = 2; means ± SD; unpaired Student's t test: *, P < 0.05; **, P < 0.01; ***, P < 0.001). **(F)** 1% CHAPSO-solubilized microsomes from HEK293/swAPP pretreated with 2.5 μM AZD3293 for 24 h (DMSO as the control) were fractionated on a Superose 6 Increase column, and fractions were incubated at 37°C for 12 h. Aβx-40 de novo generation was measured by ELISA from each fraction (n = 3; means ± SD); unpaired Student's t test: **, P < 0.01; ****, P < 0.0001. **(G)** Holo-APP and PS1-NTF immunoblots of FPLC fractions before their 37°C de novo incubation from cells treated with 2.5 μM AZD3293 or DMSO for 24 h (m, mature; im, immature; DARK, longer exposure).

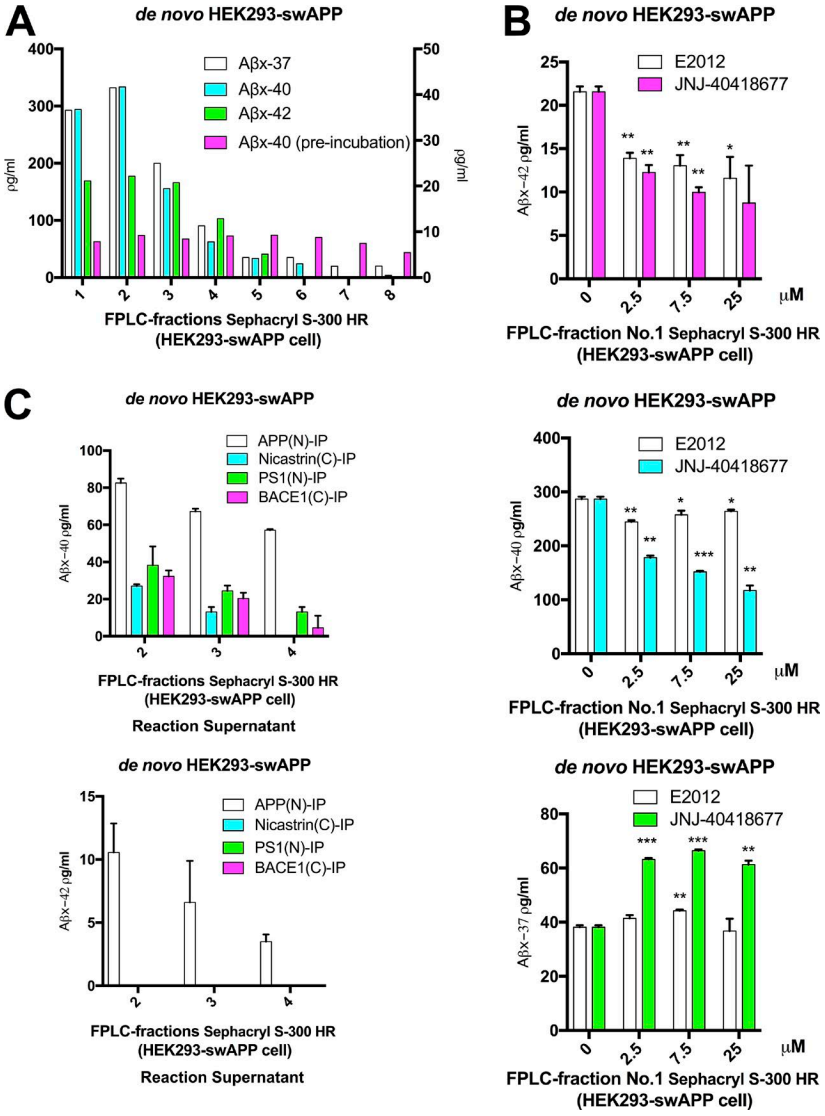

Figure 4. **De novo Aβ generation from holo-APP in immunoisolated HMW complexes. (A)** 1% CHAPSO-solubilized HEK293-swAPP microsomes were fractionated on a Sephacryl S-300 HR SEC column, and fractions #1–8 were incubated at 37°C for 12 h. Aβx-37, x-40, and x-42 de novo generation was measured by ELISA from each FPLC fraction ($n = 1$). Aβx-40 was also measured in each fraction before incubation ($n = 1$). Left y-axis, Aβx-40; right y-axis, Aβx-42 and Aβx-37. **(B)** FPLC fraction #1 was incubated at 37°C for 12 h with 2.5, 7.5, or 25 μM E2012 or JNJ-40418677. De novo Aβx-42/x-40/x-37 generation was measured by ELISA from each fraction ($n = 2$; means ± SD). Unpaired Student's *t* test: *, $P < 0.05$; **, $P < 0.01$; ***, $P < 0.001$. **(C)** IP from FPLC fractions #2–5 using four different antibodies, as indicated, was followed by incubating the immunoprecipitated beads in 500 μl reaction buffer at 37°C for 12 h. De novo Aβx-40 and x-42 generation was measured in the reaction buffer ($n = 2$; means ± SD). IPs from #5 did not generate any measurable Aβ and thus it is not shown.

Roburic acid (RA) reduces Aβ production by interfering with HMW β/γ-secretase complexes and modulating γ-secretase

Recently, the natural plant product 3-α-akebonoic acid, a pentacyclic triterpenoid acid, was reported to interrupt a putative interaction of β- and γ-secretases by binding to PS1 and thereby reducing Aβ generation without altering BACE1 or γ-secretase catalytic activities per se (Cui et al., 2015). In the context of our findings here, this report suggested the potential feasibility of pharmacologically interfering with the HMW β/γ-secretase complex to reduce Aβ generation. However, purification of 3-α-akebonoic acid from *Akebia quinata* is difficult, with very low yields of the pure product (Cui et al., 2015). We therefore searched for more abundant natural triterpenoid acids to test as potential Aβ-lowering compounds. We identified a seco derivative of pentacyclic triterpenoid acid—namely, RA (see Fig. 6 A). First, we measured total Aβ (Aβ1-x) levels in conditioned medium from HEK293/swAPP cells treated with a wide dose range of RA (50 μM down to 390 nM) for 24 h. We observed a dose-dependent decrease in Aβ secretion (Fig. 6 B). Several different mechanisms could explain reduced Aβ1-x extracellular levels from this compound: (1) decreased Aβ secretion and increased intracellular Aβ accumulation; (2) shift of cleavage from the β site (Asp1) to the β′ site (Glu11), leading to a relative increase in Aβx-40 and x-42; (3) inhibition of BACE1 leading to decreased sAPPβ and CTFβ; and (4) inhibition of γ-secretase leading to accumulated APP-CTFs. We assessed each of these possibilities. First, treatment with RA (50 μM) decreased both intracellular Aβ1-x and secretion of Aβ1-x from HEK293/swAPP cells by as much as 60% compared with DMSO alone, with LY2811376 used as a positive control for β-secretase inhibition (Fig. 6 C). This result excluded the possibility of a reduction of Aβ release into the extracellular space. Second, RA decreased both Aβx-40 and x-42 (Fig. 7 A), ruling out that the lowering of Aβ1-x represented a shift from β toward β′ cleavage or other N-terminally truncated Aβ species. Treatment with RA diminished Aβx-42 relatively more than Aβx-40 (Fig. 7 A), suggesting that RA might act in part as a GSM (see below). Purified recombinant human BACE1 was also tested to exclude the possibility that RA was a BACE1 inhibitor (Fig. 7 B). In accord, only a very high dose of RA (50 μM) decreased sAPPβ-sw production by cells (Fig. 6 D), whereas all doses of AZD3293 tested markedly lowered sAPPβ-sw secretion (Fig. 7 C), indicating no appreciable BACE1

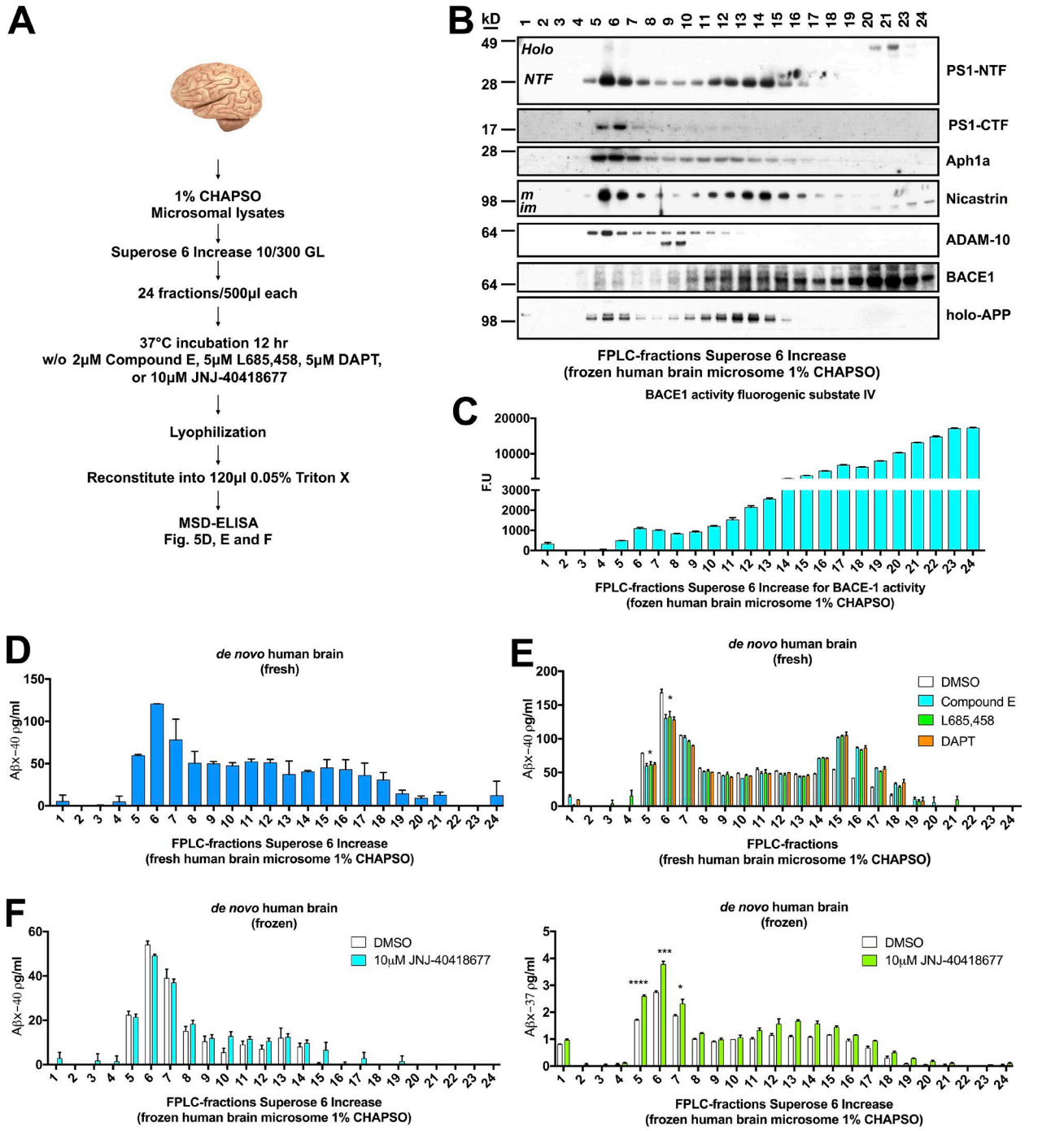

Figure 5. **De novo Aβ generation from HMW FPLC fractions of human brain lysate. (A)** Schematic of the protocol for de novo Aβ generation from human brain using fractions from the Superose 6 Increase column. **(B)** 1% CHAPSO-solubilized human brain microsomes were fractionated on the column and blotted with antibodies to the indicated proteins. **(C)** Microsomes as in B were fractionated, and each fraction was incubated at 37°C for 2 h with fluorogenic BACE1 peptide substrate IV (n = 3, means ± SD). **(D)** FPLC fractions were incubated at 37°C for 12 h. De novo Aβx-40 generation was measured by ELISA from each fraction (n = 2, means ± SD). **(E)** FPLC fractions incubated at 37°C for 12 h with indicated inhibitors and DMSO as the control. De novo Aβx-40 generation was measured by ELISA from each fraction after concentration (n = 2, means ± SD). Unpaired Student's t test: *, $P < 0.05$. **(F)** FPLC fractions were incubated at 37°C for 12 h with 10 µM JNJ-40418677 or just DMSO. De novo Aβx-40/x-37 generation was measured by ELISA from each fraction after concentration (n = 3, means ± SD). Unpaired Student's t test: *, $P < 0.05$; ***, $P < 0.001$; ****, $P < 0.0001$.

inhibition by RA. Next, WBs and ELISA showed that RA could dose-dependently lower both APP-CTFs (Fig. 6, E and F), the opposite of what γ-secretase inhibitors did (Figs. 6 E and 7 D). Having ruled out these four possible mechanisms for Aβ-lowering by RA, we asked whether RA instead altered the newly identified HMW β/γ-secretase complex.

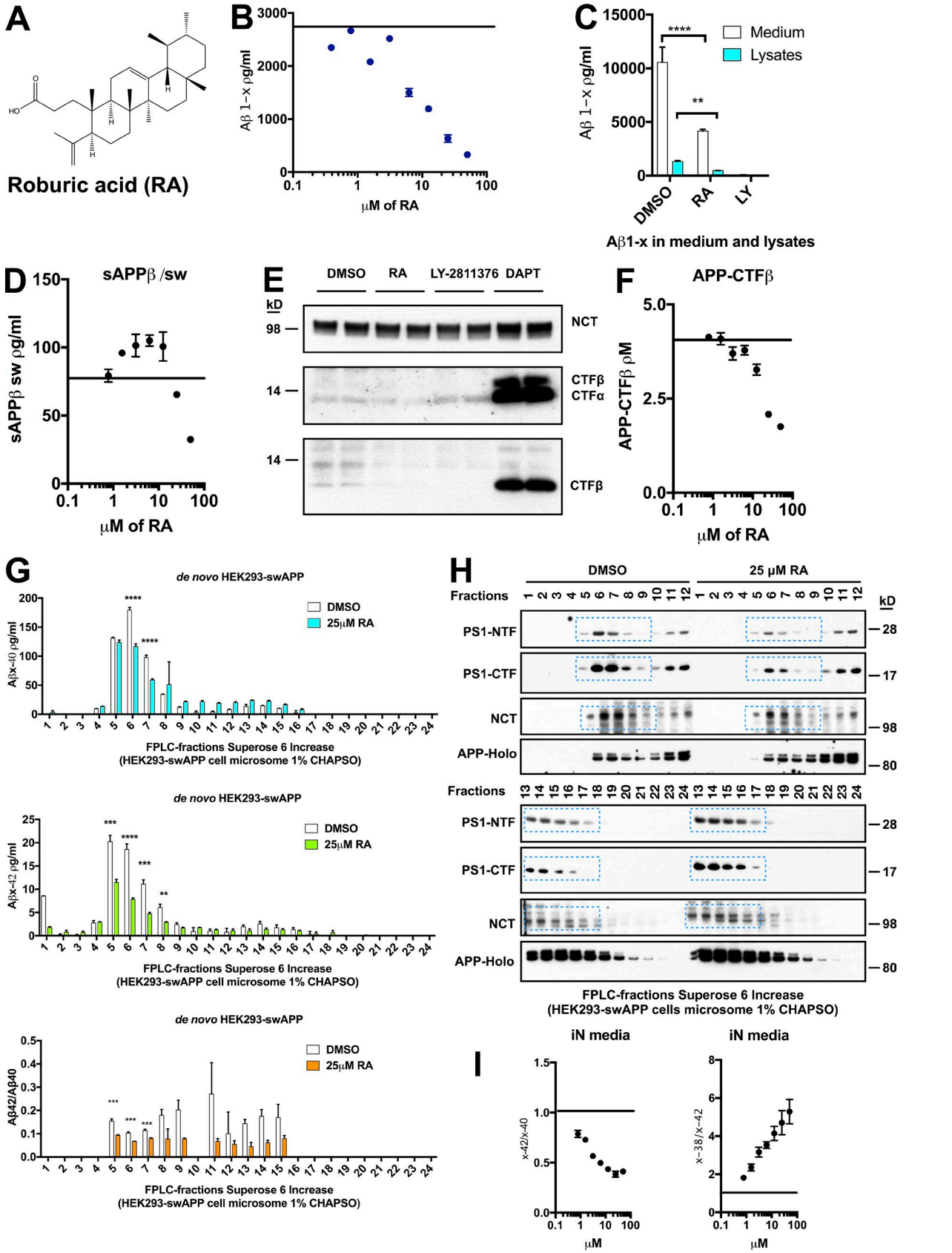

Figure 6. **RA destabilizes the HMW β/γ complex and modulates γ-secretase activity to reduce Aβ production. (A)** The structure of RA. **(B)** Aβ1-x in medium measured by ELISA after 24-h treatment of HEK293-swAPP cells with RA (dosages from 390 nM to 50 μM; *n* = 2, means ± SD; some error bars too small to be visible). Black line, Aβ1-x level with plain DMSO treatment. **(C)** Extracellular and intracellular Aβ1-x were measured by ELISA after 24-h treatment of HEK293-swAPP cells with 50 μM RA, with DMSO and 10 μM LY2811376 (LY) as controls (*n* = 6, means ± SD). Unpaired Student's *t* test: **, P < 0.01;

FPLC fractions (Superose 6 Increase column) from HEK293-swAPP cells that had been treated with RA (25 µM) were assayed for de novo Aβ generation. RA significantly reduced Aβx-40 generation by HMW fractions #6 and 7 and Aβx-42 generation by HMW fractions #5–7 (Fig. 6 G). Notably, the Aβx-42/40 ratio was also decreased significantly in HMW fractions #5–7 (Fig. 6 G). Immunoblots of all FPLC fractions before the de novo Aβ generation showed that RA had decreased PS1-NTF, PS1-CTF, and NCT levels in HMW fractions #6 and 7, with a parallel increase in LMW fractions #13–16 (Fig. 6 H). Thus, RA appeared to decrease Aβ production by redistributing the γ-secretase catalytic components from the Aβ-competent HMW complex to an LMW fraction that generates little or no Aβ (Fig. 6, G and H). We assayed microsomes from total (unfractionated) cell lysates for BACE1 activity with the fluorogenic substrate: there was no difference in BACE1 activity between RA- and DMSO-treated cells (Fig. 7 E). However, when we assayed BACE1 activity across all FPLC fractions, RA significantly reduced fluorogenic peptide cleavage in fractions #5, 6, and 8–13 (Fig. 7 F), among which fractions #5 and 6 had been shown to have the most HMW β/γ-secretase complexes contributing to Aβ production (Fig. 3 C). In contrast, RA treatment caused no change in BACE1 peptide cleavage activity in the BACE1-rich LMW fractions (Fig. 7 F). We conclude that RA lowers Aβ production by decreasing both the levels of γ-secretase components (PS1-NTF/PS1-CTF/NCT) and BACE1 proteolytic activity present in the HMW complexes.

RA reduced Aβx-42 more than Aβx-40 (Fig. 7 A), which is different than that reported for the related pentacyclic triterpenoid acid, 3-α-akebonoic acid (Cui et al., 2015). This suggested that RA might also be able to modulate γ-cleavage. We therefore treated HEK293-swAPP cells with RA (versus DMSO) in serial doses from 50 µM down to 390 nM for 24 h and measured four distinct Aβ species in the conditioned medium (Fig. 7 G). (Aβx-43 was only detectable in the DMSO-treated medium [not shown].) We measured an IC_{50} of <3 µM for Aβx-42, ∼20 µM for Aβx-40, and ∼6 µM for Aβx-37, whereas most doses increased Aβx-38 (Fig. 7 G). Next, we applied the same RA treatment to iPSC-derived, neurogenin-induced human neurons (iN cells) and obtained closely similar findings (Fig. 7 H). RA decreased Aβx-42 by 50% at 3.125 µM and increased Aβx-38 by 50% at this dose. Aβx-40 was barely changed, and Aβx-37 was decreased as RA dosage increased. After normalizing the Aβx-42/x-40 and the Aβx-38/x-42 ratios (Fig. 6 I), we observed a clear, dose-dependent decrease in Aβx-42/x-40 ratio and increase in Aβx-38/x-42 ratio, suggesting that RA modulates γ-activity. However, RA is unique compared with several other GSMs we tested: acidic GSMs (such as sulindac sulfide) would increase the Aβx-38/x-42 ratio without changing x-40; nonacidic GSMs (such as E2012) would increase both Aβx-38 and x-37 with reduced x-42 and x-40 (Crump et al., 2013). Our above comparison of RA to β-secretase inhibitors (BSIs), γ-secretase inhibitors (GSIs), and GSMs suggests that the mechanism of RA does not fall cleanly into any of these categories.

β/γ-Secretase complexes isolated from cells expressing familial Alzheimer's disease (FAD) mutant PS1 generate an Aβ pathogenic profile indistinguishable from that of whole cells

We explored the proteolytic activities of β/γ-secretase HMW complexes harboring FAD PS1 mutations. Using two sets of HEK293 cell lines overexpressing either WT-APP or swAPP as substrates, we quantified the effects on Aβ generation of two FAD PS1 mutations Y115H (Alzheimer's disease onset at 35–47 yr) and L286V (Alzheimer's disease onset at 47–50 yr; Citron et al., 1997, 1998). Cell lines expressing swAPP have much more Aβ secretion than cells expressing WT-APP: the secreted Aβx-40 level from a WT-APP/WT-PS1 cell line was 246.2 ± 18 pg/ml and from a swAPP/WT-PS1 line was 2318 ± 49.2 pg/ml (means ± SD; n = 3 each). We used FPLC fractions (Superose 6 Increase column) from HEK293 cells stably overexpressing WT or FAD mutant PS1 with WT or swAPP to measure de novo Aβ generation at 37°C (Fig. 8, A and B). The HMW β/γ-secretase complexes having mutant PS1 generated a different profile of Aβ peptides than those having WT PS1, as reflected by the Aβx-42/x-40 ratio. We measured the cell-secreted Aβx-42/x-40 ratio in 24-h conditioned medium from these cells and averaged the de novo Aβx-42/x-40 ratios from FPLC fractions #5–17 to make a comparison (Fig. 8, C and D). The Aβx-42/x-40 ratios derived from secreted Aβ in whole-cell medium (Fig. 8 D) and that from de novo Aβ production from the FPLC fractions (Fig. 8 C) were closely similar. These results suggest that the HMW β/γ-secretase complexes serve as the major source of Aβ secretion, and they also demonstrate the clear clinical relevance of the HMW β/γ complexes, as they produce a FAD-PS1 pathogenic profile of Aβ peptides that is indistinguishable from that of the respective whole cells.

Colocalization of BACE1 and γ-secretase shown by proximity ligation assay (PLA) and stimulated emission depletion (STED) nanoscopy

To support our biochemical findings, we first performed confocal immunofluorescence microscopy on HEK293 cells that express only endogenous β- and γ-secretases. Confocal imaging showed fine punctate staining for BACE1 and PS1 throughout the cell (Fig. 9 A), with the strongest colocalization in the perinuclear region. To confirm this apparent colocalization between BACE1 and PS1, we employed a highly sensitive and quantitative in situ PLA to visualize the endogenous BACE1–PS1 complexes, with TfR/PS1 as a negative control. Superior to most other colocalization

****, P < 0.0001. **(D)** sAPPβ-sw secretion from the same cell line, measured by ELISA after 24-h treatment with increasing doses of RA with DMSO (black line) as the control (n = 3, means ± SD; some error bars are too small to be visible). **(E)** Immunoblots of lysates from the same cell line treated for 24 h with 50 µM RA, with DMSO or 10 µM LY2811376 or 10 µM DPAT as the control. **(F)** Intracellular APP-CTFβ was quantified by ELISA after 24-h treatment with RA or DMSO (black line; n = 4; means ± SD; some error bars are too small to be visible). **(G)** Microsomes from same cell line pretreated with 25 µM RA for 24 h (DMSO as the control) and fractionated on the Superose 6 Increase column. Fractions were incubated at 37°C for 12 h. De novo Aβx-40/x-42 generation was measured by ELISA, and an Aβx-42/x-40 ratio was plotted (n = 3, means ± SD). Unpaired Student's t test: **, P < 0.01; ***, P < 0.001; ****, P < 0.0001. **(H)** FPLC fractions before de novo incubation were blotted with antibodies to the indicated proteins. **(I)** Normalized Aβx-42/40 and Aβx-38/42 ratios in iN cells treated with increasing doses of RA, with DMSO set at 1 (n = 6, means ± SD; some bars are too small to be visible).

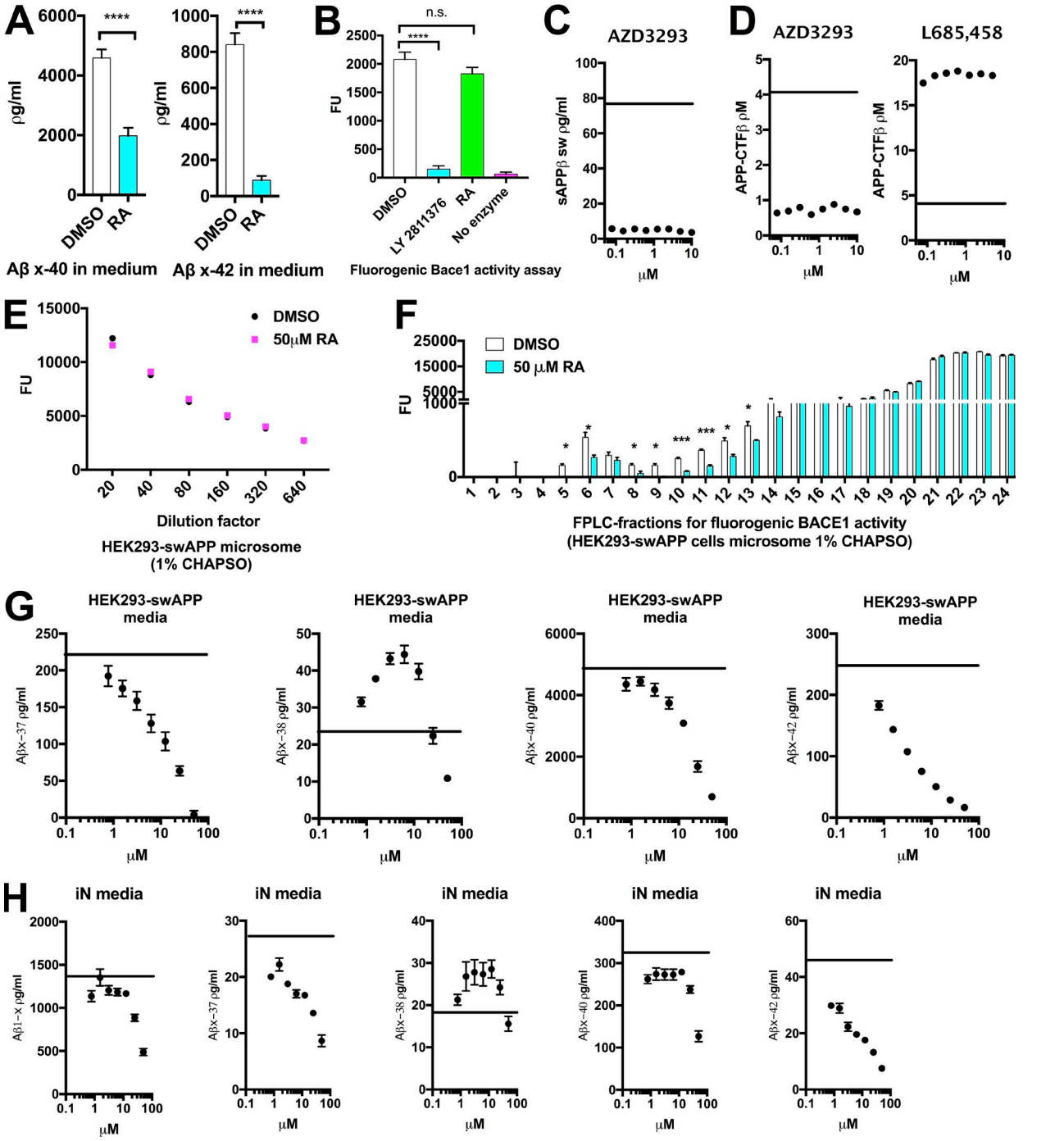

Figure 7. **RA does not inhibit BACE1 or γ-secretase. (A)** Aβx-40 and Aβx-42 were measured in 24-h conditioned medium after treating with 50 μM RA or DMSO (n = 6, means ± SD). Unpaired Student's t test: ****, P < 0.0001. **(B)** 500 ng recombinant BACE1 with 50 μM RA or 10 μM LY2811376 and DMSO as the control were tested using a fluorogenic BACE1 activity assay (n = 3, means ± SD; unpaired Student's t test: ****, P < 0.0001). Fluorogenic substrate alone was used as a blank control. **(C)** sAPPβ-sw were measured by ELISA after 24-h treatment of increasing doses of AZD3293, with DMSO as the control (black line; n = 1). **(D)** Intracellular APP-CTFβ quantified by ELISA after 24-h treatment with increasing doses of AZD3293 or L685,458, with DMSO as the control (black line; n = 1). **(E)** 1% CHAPSO-solubilized microsomes from the same cell line treated with DMSO or 50 μM RA were diluted 20–640 times and incubated with fluorogenic BACE1 substrate IV, and activity was measured (n = 1). **(F)** 1% CHAPSO-solubilized microsomes from same cell line treated with DMSO or 50 μM RA and then fractionated on a Superose 6 Increase column. BACE1 activity was measured as in E (n = 3, means ± SD; unpaired Student's t test: *, P < 0.05; ***, P < 0.001). **(G)** Aβx-37, x-38, x-40, and x-42 were measured by ELISA after 24-h treatment with increasing doses of RA, with DMSO as the control (black line) on HEK293-swAPP cells (n = 4, means ± SD; some error bars are too small to be visible). **(H)** Aβ1-x, x-37, x-38, x-40, and x-42 in medium measured by ELISA after 24-h treatment with RA on D23 iN cells with serial of doses from 50 μM to 390 nM (n = 6, means ± SD; some error bars are too small to be visible; black line, DMSO).

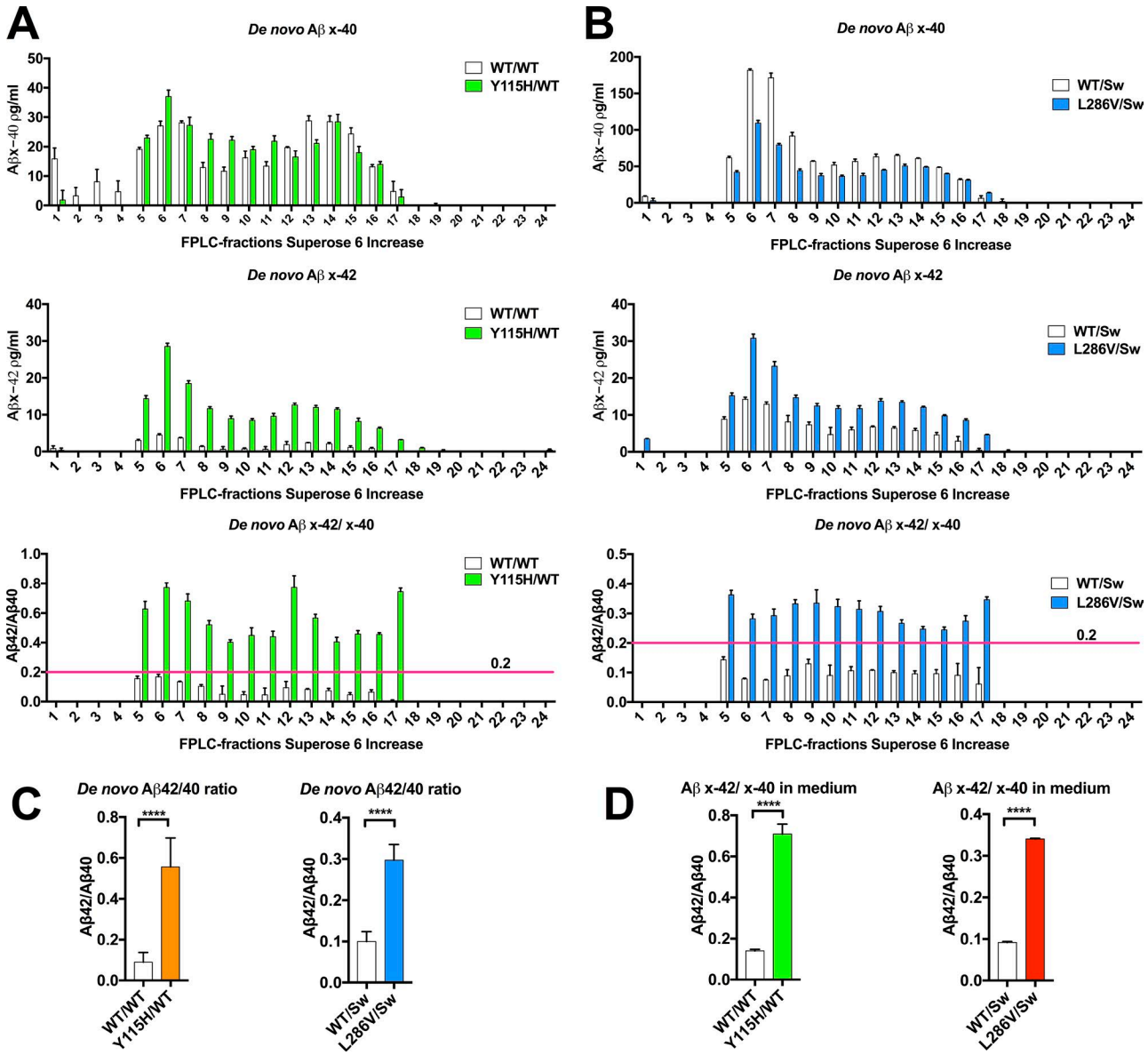

Figure 8. **De novo Aβ generation closely reflects whole-cell Aβ secretion in both WT PS1- and FAD mutant PS1-expressing cells. (A and B)** 1% CHAPSO-solubilized microsomes prepared from the indicated HEK293 cell lines were fractionated on a Superose 6 Increase column, and fractions #1–24 were incubated at 37°C for 12 h. De novo Aβx-40/x-42 generation was measured by ELISA from each fraction after concentration (n = 3; means ± SD). **(C)** The average de novo Aβx-42/x-40 ratio of fractions #5–17 from the indicated cell lines. **(D)** Secreted Aβx-42/40 ratio in 24-h conditioned medium from the same cells as in C (n = 3, means ± SD; ****, P < 0.0001).

methods, PLA requires a maximum distance of 40 nm between two labeled proteins to produce a signal (Fig. 9, B and C). Quantification of PLA signals showed that BACE1–PS1 association (<40 nm) is significantly more prevalent than TfR/PS1 association (Fig. 9 D). Finally, we used a superresolution STED nanoscope to visualize endogenous BACE1–PS1 complexes in HEK293 cells. We observed perinuclear colocalization of BACE1–PS1 (Fig. 9 E, upper panels), and these colocalized puncta (diameter ∼150 nm) were clearly visualized under STED depletion, having a resolution as high as 14 nm per pixel (Fig. 9 E, lower panels). All three imaging methods, taken together with our extensive biochemical data, document the occurrence of β/γ-secretase complexes in vivo, in vitro, and in situ.

Discussion

The discovery of the normal cellular production of Aβ via an apparent intramembrane cleavage of APP (Haass et al., 1992; Seubert et al., 1992; Shoji et al., 1992) provided the first evidence of the unusual hydrolysis of peptide bonds within the lipid bilayer, and the parallel discovery of the intramembrane cleavage of SREBP by Site-2 protease (Rawson et al., 1997) led to the recognition of RIP as a general biological process (Brown et al., 2000). Because many single-transmembrane substrates, including Notch and its ligands, are now known to require endoproteolysis by α- or β-secretase followed by γ-secretase, understanding the process underlying these sequential cleavages is fundamental to cell biology. In particular, identification of the biochemical

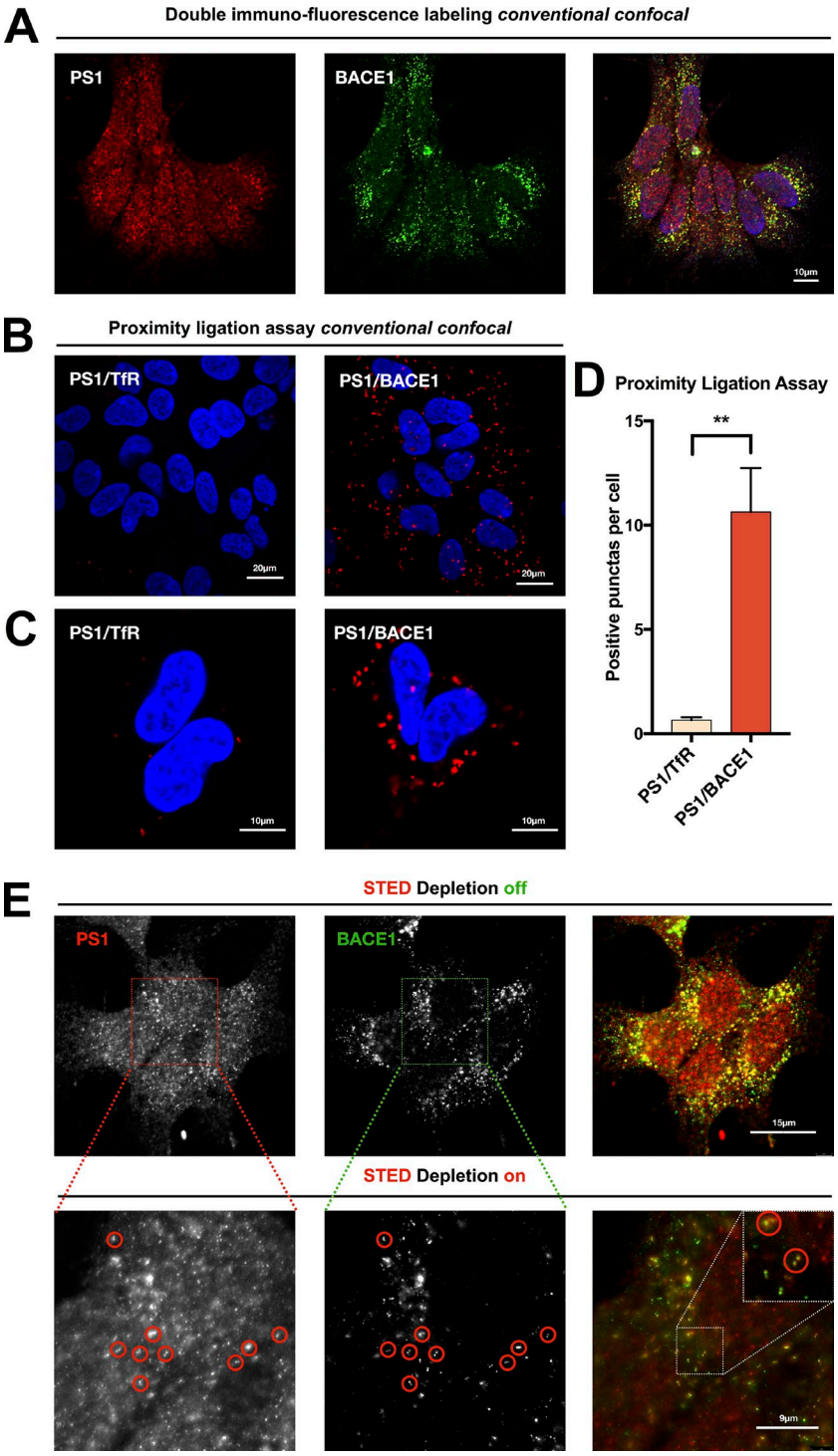

Figure 9. **Confocal microscopy, PLA, and analysis by STED nanoscope of BACE1 and γ-secretase colocalization in HEK293 cells. (A)** 1-µm optical section of HEK293 cells stained for BACE1 (green), PS1 (red), and DAPI (blue), viewed by confocal microscopy. **(B)** In situ PLA staining, showing interactions between BACE1/PS1 or TfR/PS1 signals (red) and DAPI (blue) by confocal microscopy, low magnification. **(C)** High magnification of B. **(D)** Quantification of PLA signals from five frames of images each (red puncta) between BACE1/PS1 (119 cells), with TfR/PS1 (106 cells) as a negative control. Unpaired Student's *t* test: $n = 5$, mean ± SEM; **, $P < 0.01$. **(E)** Superresolution STED images of BACE1 (green) and PS1 (red) immunoreactive puncta in HEK293 cells. Some examples of colocalized puncta are marked with red circles.

mechanism by which holo-APP is cleaved sequentially to Aβ peptides is needed to design safe and effective inhibitors and modulators of this process in order to treat and ultimately prevent a major portion of age-related cognitive decline.

Here, we describe the existence of a hitherto unrecognized HMW complex that processes full-length transmembrane proteins (e.g., APP) by β- and γ-secretases to final products (Aβ peptides) in cultured cells and human brain. We show that Aβ generation by the HMW complex can be modulated by small molecules, including known GSMs, but also by the intriguing new modulator, RA, which lowers Aβ generation by redistributing the γ-components from the Aβ-competent HMW complex to lower MW inactive fractions without directly inhibiting β- or γ-secretase. We also conducted immunocytochemical analyses of the endogenous β/γ interaction using PLA and the superresolution STED nanoscope to confirm our biochemical findings and provide evidence of an interaction between BACE1 and PS–γ-secretase in situ. Together with our previous work on a multiprotein complex of the α- and γ-secretase enzymes (Chen et al., 2015), our collective findings support a novel model of RIP that

involves functional collaboration between a sheddase and an intramembrane protease within the same physical complex in order to mediate rapid, sequential proteolysis of a substrate in an efficient manner.

We initially observed that endogenous BACE1 could be coimmunoprecipitated with γ-secretase from CHAPSO-solubilized mouse brain microsomes. A second method, nondenaturing FPLC, showed that BACE1 and the mature γ-components of mouse brain eluted together in certain HMW fractions sized at >5 MD. The endogenous β- and γ-secretases could be coimmunoprecipitated from such HMW FPLC fractions but not from LMW FPLC fractions that contain abundant BACE1 but no mature (PS heterodimeric) γ-secretase. The identification of α/γ and separately β/γ-secretase complexes suggests the apparent existence of a heterogeneous array of high-order protease complexes that are independent; we have not been able to detect a complex containing the two sheddases and γ-secretase (see Fig. 10, C and D, in Chen et al., 2015).

As regards function, we found that the HMW β/γ complex is able to mediate sequential cleavages of the full-length APP protein into Aβ peptides. Using FPLC fractions prepared from cultured cells or normal human brain, we detected de novo Aβ generation at 37°C from holo-APP substrate that is apparently docked in the HMW protease complex, whereas this did not occur in LMW FPLC fractions, as expected, because they are rich in BACE1 protein but lack γ-secretase. The array of C-terminally heterogeneous Aβ peptides generated from these HMW fractions was appropriately altered by GSMs, by BACE1 inhibitors, and by RA, but could not be inhibited by active site directed γ-secretase inhibitors, presumably because the β/γ complex already contained bound holo-APP (and other γ-substrates) that precluded efficient entry of an inhibitor into the γ-secretase active site. As our recent work showed (Bolduc et al., 2016a), NCT functions as a gatekeeper to prevent holo-APP from entering into the final PS–γ-secretase catalytic site without first undergoing ectodomain shedding by α- or β-secretases. We postulate that NCT is the gatekeeper for holo-substrate but not for APP-CTF once the ectodomain has been shed by BACE1. Our data thus suggest that the HMW complexes can contain mature β and γ proteases complexed with substrate (APP), as illustrated in Fig. 10 A. De novo Aβ42 and 40 peptides were generated from the FPLC-isolated β/γ complexes at the normal ratio of 0.1–0.2, in accord with these complexes serving as the principal source of physiological Aβ peptides made by cells.

Importantly, coIPs of HMW FPLC fractions using antibodies specific for holo-APP, PS1, NCT, or BACE1 were each incubated at 37°C to generate the same array of Aβ peptides as we observed in the input FPLC fractions and culture medium. However, the coIP of APP generated more Aβ products than the coIP of BACE1 or the γ-components, which suggests that the IP of APP enriches for complexes that are already loaded in part with holo-APP and thus yield more APP products than pulling down via the secretases, which presumably interact with other substrates besides APP.

Numerous cofactors of γ-secretase have been reported (e.g., Chen et al., 2006; Wakabayashi et al., 2009), and a catalytically active γ-secretase complex is thought to be larger (>2 MD) than the MW of its four essential components combined (~250 kD; Li et al., 2000a; Farmery et al., 2003). In previous studies, (1) a recombinant substrate (such as APP-C99 or ΔE-Notch) was used to demonstrate γ-activity in vitro (Li et al., 2000a); (2) overexpression of the γ-components was required to purify γ-secretase (Fraering et al., 2004b; Cacquevel et al., 2008; Wakabayashi et al., 2009); and (3) immobilized TSA inhibitors were used to isolate endogenous γ-secretase (Li et al., 2000b; Esler et al., 2002). In the current study, the de novo Aβ generation we observed is specifically derived from the HMW β/γ-complex since (1) an endogenous substrate (APP) present within the HMW complex was used to evaluate γ-activity; (2) an endogenous protease complex was isolated and characterized from both cells and normal human brain; (3) the HMW complex cleavage activity was sensitive to GSMs but not GSIs, thus distinct from the γ-secretase pulled down by a TSA; and (4) the higher de novo Aβ generation by this complex after initially inhibiting BACE1 demonstrated the existence of complexes having holo-APP protein docked and ready for sequential processing. Given these special properties, it is reasonable that the β/γ complex has not been previously discovered in conventional protein–protein interaction screens used heretofore. Indeed, conventional protein–protein interaction screens mostly failed to detect substrates such as APP holo-protein, suggesting that many pulled-down γ-secretase complexes may lack docked substrates.

To further strengthen our findings, we examined RA in our experimental system in an attempt to disrupt active β/γ complexes and reduce Aβ generation. After characterizing RA as an Aβ-lowering agent distinct from BSIs, GSIs, and GSMs, we showed that RA could decrease de novo Aβ generation in the HMW FPLC fractions by lowering PS1-NTF and BACE1 levels in those Aβ-generating fractions and shifting them to LMW fractions, which suggests that HMW β/γ complexes may be disassembled in part by RA, thereby precluding efficient Aβ generation.

In cultured cells or brain tissue, one can routinely detect endogenous APP-CTFs. In this regard, we observed APP-CTFβ in LMW fractions (Figs. 3 A and S3 C) that cannot support de novo Aβ production upon incubation at 37°C (Fig. 3 C). It is possible that sheddases such as BACE1 could shed holo-substrate by two modes: with or without immediate γ-secretase cleavage. We speculate that there may be two broad substrate processing pathways: for ectodomain shedding (extracellular signaling) and for sequential processing (both extra- and intracellular signaling; Fig. 10 B). In this case, endogenous APP-CTFs observed in cells at steady state could be byproducts of the principally ectodomain-shedding pathway, with the resultant CTFs turned over in a non–Aβ-generating pathway such as in lysosomes and by autophagy (Tian et al., 2013). Such speculations are not unreasonable, as sAPP-β, Aβ, and AICD are believed to have different physiological roles in the central nervous system (Reinhard et al., 2005; Chasseigneaux and Allinquant, 2012). Moreover, the discovery of η-secretase for APP processing appears to provide an example of a principal ectodomain shedding event (see Fig. S2 D).

In summary, our collective findings establish the physical and functional association of α- or β-secretase with γ-secretase, providing an efficient mechanism for processing many single-transmembrane substrates to enable diverse signaling, protein turnover, and other functions. The HMW β/γ complexes we identify are the principal generators of cellular Aβ, both

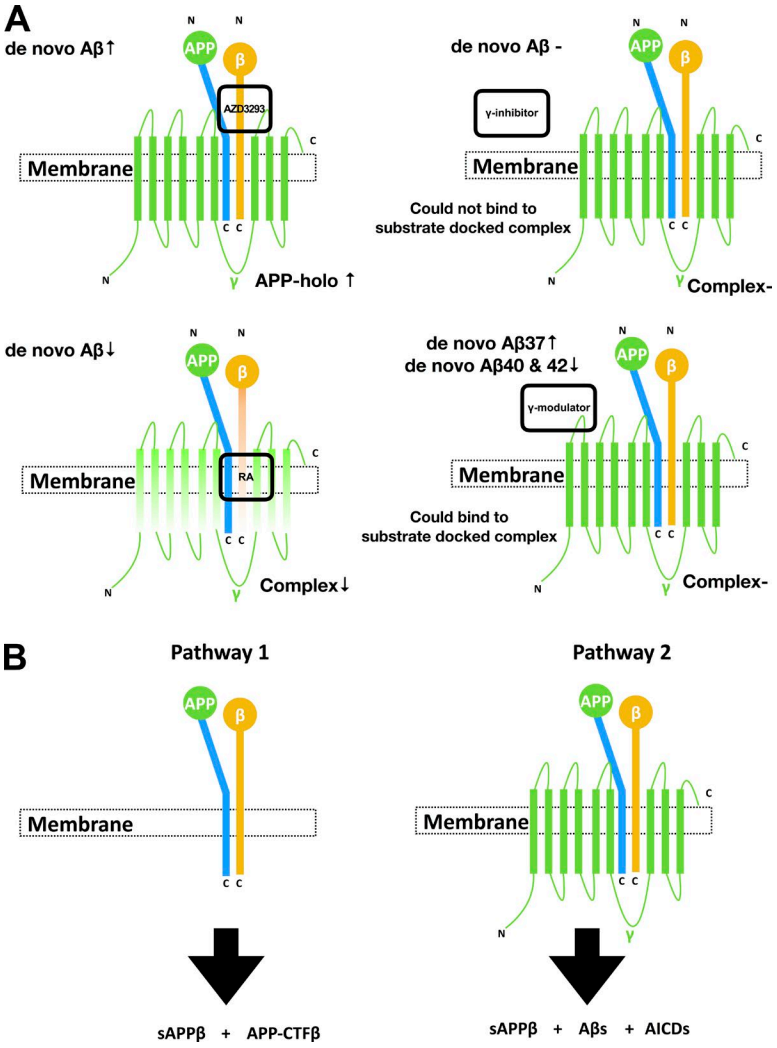

Figure 10. **Schematic illustration of the mechanism of the HMW β/γ secretase complex. (A)** Summary illustration of HMW complexes and the effects of different compound treatments. **(B)** Two potential pathways of membrane-shedding events: principally ectodomain shedding and principally sequential substrate cleavages.

quantitatively and qualitatively. Screening these isolated complexes in vitro for compounds like RA that appear to decrease the interaction of the two secretases without inhibiting either of them represents a novel therapeutic approach for Aβ lowering that is complementary to the current search for safe and effective β-secretase inhibitors or GSMs.

Materials and methods

Reagents

LY2811376, AZD3293, DAPT, and L-685,458 were from Selleckchem; β-secretase inhibitor IV, Compound E, and β-secretase substrate IV (fluorogenic) were from Millipore; RA and JNJ-40418677 were from Aobious; E2012 was from APExBIO; synthetic Aβ peptides were all from Anasepc; and recombinant human BACE l protein was from R&D Systems.

Cell culture

HEK293 cells were maintained in standard medium: DMEM plus 10% FBS, 2 mM L-glutamine, 100 µg/ml streptomycin, and 100 IU/ml penicillin. For our HEK293/swAPP cell line, which overexpresses human swAPP, standard medium was supplemented with G418. For our HEK293 coexpressing APP and PSEN1, standard medium was supplemented with G418 (APP) and Zeocin (PS1). For the Neurogenin 2-iN (iN) differentiation, iPSCs were differentiated following the protocol of Muratore et al. (2017). Cultures were treated with doxycycline (2 mg/ml) on day 1 to induce differentiation, fed with a series of medium changes, treated at day 23, and harvested at day 24.

Mice

All experiments involving mice were approved by the Harvard Medical School Committee on Animals. Both male and female C57BL/6 mice were used. Animals were housed in a temperature-controlled room on a 12-h light/12-h dark cycle and had free access to food and water.

BACE1 KO cell generation and transfections

Homozygous human BACE1-KO HEK293 cell lines were generated using a CRISPR/Cas9 nuclease-mediated system. The guide RNAs were designed using the CRISPR Design software package (http://crispor.tefor.net/) to minimize potential off-target effects. Two oligonucleotides (capitalized characters represent target sequence on human BACE1 exon 3), 5′-caccGGCCATGGGGGA TGCTTACC-3′ and 5′-aaacGGTAAGCATCCCCCATGGCC-3′, were annealed and ligated into vector PX459 (Ran et al., 2013; 62988;

Addgene) to express one gRNA targeting BACE1. After transfection of PX459 into HEK293/swAPP cells for 48 h, puromycin selection was undertaken for 1 wk. BACE1 KO cells were isolated via limiting dilution cloning and confirmed by WB and ELISA. For test of chimera-BACE1 experiments, Xfect Transfection Reagent (Clonetech) was used according to the manufacturer's protocol. Culture medium was changed 24 h after transfection for conditioning. 24-h conditioned medium and cell lysates were harvested for ELISA or coIP.

Mutagenesis

TMD-swapped mutants of BACE1 were cloned into a pcDNA3.1(+), using a two-step PCR. A total of four primers were used per construct: N/C-terminal primers 5′-ttagaattcatggcccaagccctgccctgg-3′ and 5′-ttactcgagttaaacgtgatggtgatggtgatgcttcagcaggagatgt-3′ and internal primers 5′-TGCATCCTGTCCCTCTGCATCCTGGTGCTGGTCTACACCATCTTCcagtggcgctgcctc-3′ and 5′-CACCAGGATGCAGAGGGACAGGATGCAGGGGATGACCACGGCCACggtcatgagggttga-3′, which contained the desired mutation in-frame (capitalized characters represent the MT5-MMP TMD sequence) with the adjacent BACE1 sequence. In the first round of PCR, two reactions would generate a 5′- and a 3′-half with a complementary 27-bp overlap containing the desired mutation. The two resulting products were added together and used as a template for the second round of PCR, where extreme N/C-terminal BACE1 primers were added. All mutants were generated in BACE1 isoform with a C-terminal 6xHis tag, and their sequences were verified.

Human brain

A human temporal cortex specimen was obtained through collaboration with the neuropathology department at Brigham and Women's Hospital under institutional review board–approved protocols. The sample came from brains that were removed and directly used in our experiments to isolate microsome fractions.

Microsome preparations from cultured cells and brain sample

For microsome preparations from cultured cells, cells were first Dounce homogenized with a tight pestle in TBS containing no detergent with 15 strokes, followed by passage through a 27.5-gauge needle four times. Samples were then centrifuged at 1,000 *g* followed by a 100,000-*g* ultracentrifuge spin to pellet microsomes, which were solubilized in 50 mM Hepes buffer, 150 mM NaCl, containing 1% CHAPSO or 0.5% DDM for 60 min, followed by another 100,000-*g* spin. For microsome preparations from brain samples, fresh sample (1 g) was chopped into small pieces with a razor blade, and then homogenized with 15 strokes of a Dounce glass homogenizer (Fisher) in 4 ml of 0.32 M sucrose, 10 mM Hepes, pH 7.4, 1 mM EDTA, and protease inhibitors. Brain homogenate was centrifuged two times at 1,500 *g* for 10 min each to discard nucleus and debris. Supernatant was then centrifuged at 100,000 *g* at 4°C in a TLA 100.3 rotor (Beckman Coulter) for 30 min to pellet microsome fractions, which were solubilized in 50 mM Hepes buffer, 150 mM NaCl, containing 1% CHAPSO for 60 min, followed by another 100,000-*g* spin. Protein concentrations were determined for both lysates and microsomes by a bicinchoninic acid protein assay (Thermo Fisher Scientific), and all samples were normalized for equal concentration before experiments.

CoIP

0.25% or 1% CHAPSO solubilized microsomes or FPLC fractions were precleared with protein G–Sepharose for 1 h, and the resulting supernatants were incubated with the appropriate antibody for 1 h at 4°C. The immunoprecipitates were incubated with protein G–Sepharose overnight at 4°C and then washed three times in lysis buffer. The immunoprecipitated proteins were then eluted in SDS sample buffer for immunoblots or otherwise specified. To eliminate IgG heavy/light chain bands on immunoblots, signals were detected with HRP-conjugated bio-nanocapsules incorporating IgG Fc-binding Z domains derived from *Staphylococcus aureus* protein A (Beacle) instead of the secondary antibody. The antibodies used to precipitate specific antigens were for Integrin αl, AB1934 (rabbit, RRID: AB_302689; Millipore); for Integrin α2, AB1936 (rabbit, RRID: AB_2265143; Millipore); for Integrin β1, AB1952 (rabbit, RRID: AB_91150; Millipore); for mBACE1, PA 1-757 (rabbit, RRID: AB_325863; Thermo Fisher Scientific); for hBACE1, poly8401 (rabbit, RRID: AB_2565445; BioLegend); for hBACE1, poly8402 (rabbit, RRID: AB_2565446; BioLegend); for NCT, N1660 (rabbit, RRID: AB_477259; Sigma-Aldrich); for PS1-N, PRB-354P (rabbit, RRID: AB_389690; BioLegend); for APP-N, MAB348 (mouse, RRID: AB_94882; Millipore); for Aph-1b, ab24613 (rabbit, RRID: AB_2058221; Abcam); for Bip, 610978 (mouse, RRID: AB_398291; BD Biosciences); for TfR, 612124 (mouse, RRID: AB_399495; BD Biosciences), and for His-tag, 652502 (mouse, RRID: AB_11204427; BioLegend).

Electrophoresis and WB

Samples were loaded onto 4–12% or 8% Bis-Tris gels using MES-SDS or MOPS-SDS running buffer (Invitrogen), transferred to nitrocellulose membranes, and probed for various proteins using standard WB. The resultant blots were detected with ECL and exposure to film. The antibodies used to detect specific antigens were, for mBACE1, EPR19523 (rabbit; Abcam); for hBACE1, D10E5 (rabbit, CST, RRID: AB_1903900); for ADAM10, MABN1123 (rabbit, RRID: AB_10972023; Abcam); for MT5-MMP, GTX128246 (rabbit; Genetex); for Meprinβ, PA5-47474 (rabbit, RRID: AB_2607364; Thermo Fisher Scientific); for PS1-N, SC-7860 (rabbit, RRID: AB_2170581; Santa-Cruz); for PS1-C, EP-2000Y (rabbit, RRID: AB_1310605; Abcam); for PS2-C, EP-1515Y (rabbit, RRID: AB_882202; Abcam); for NCT, SC-14369 (goat, RRID: AB_2282503; Santa-Cruz); for Aph-1aL, PRB-550P (rabbit, RRID: AB_291682; BioLegend): for SPP, ab16080 (rabbit, RRID: AB_302242; Abcam); for SPPL2b, PA5-42683 (rabbit, Abcam RRID: AB_2606446; Abcam); for APP-CTF, C-7 (rabbit, homemade); for APP (573–596), SIG-39180 (mouse, RRID: AB_10719734; BioLegend); for mAPP (597), 28055 (rabbit, RRID: AB_918338; IBL); for APP-CTF (asp1), 3D6 (mouse, homemade); for LRP1, ab92544 (rabbit, RRID: AB_2234877; Abcam); for APLP1, W1CT (rabbit, homemade); and for RHBDL2, 12467-1-AP (rabbit, RRID: AB_11232403; Proteintech).

2D BN/SDS-PAGE

Cultured cells or brain microsomes were lysed in a lysis buffer containing 1% CHAPSO or 0.5% DDM. After preclearing lysates

by ultracentrifugation at 100,000 *g* for 30 min, lysates mixed with native sample buffer (Thermo Fisher Scientific) and CBB G-250 (up to 1/4 of detergent concentration in each sample) were loaded on Native 3–12% Bis-Tris gel. After 150 min running at 150 V was done at 4°C, strips of gel were cut vertically and incubated with 50 mM DTT and 1% SDS for 2 h at 37°C. Presoaked strips were placed for the second dimension in Novex Bis-Tris gels with 2D wells, and electrophoresis was done using MES-SDS running buffer for an LMW target and MOPS-SDS running buffer for an HMW target.

FPLC

Microsomes isolated from culture cells, normal mouse brains, and human brain were solubilized in 1% CHAPSO (350 µl or 3.5 ml of total volume), injected onto a Superose 6 Increase 10/300 column (24-ml bed volume) or a HiPrep 16/60 Sephacryl S-300 HR (120-ml bed volume), and run on an FPLC system (AKTA purifier; GE Healthcare) in 50 mM Hepes buffer, 150 mM NaCl, and 0.25% CHAPSO, pH 7.4. 500/2,000-µl fractions were collected for downstream experiments. Columns were calibrated with Gel Filtration Standard (Bio-Rad), which ranges from 1,350 to 670,000 D.

β-Secretase activity assay (fluorogenic)

For FPLC fractions, sodium acetate was added to each fraction for a final concentration of 10 mM. 50-µl reaction buffer (10 mM sodium acetate, 1.5 mM NaCl, 0.1% Triton X-100, and 0.32 M sucrose, pH 5.0) containing 20 µM fluorogenic substrate IV (565758; Millipore) was added to 50 µl of adjusted FPLC samples. For immunoprecipitated samples, Sepharose beads were incubated in extraction buffer from a commercial β-secretase activity assay kit (565785; Millipore) on ice for 30 min and spun at 6,000 *g* briefly. 50 µl supernatant was mixed with 50 µl reaction buffer containing 20 µM fluorogenic substrate IV. In both cases, reactions were incubated at 37°C for 2 h, and fluorescence signals were read at excitation 335 nm/emission 490 nm on a plate reader (Synergy H1, BioTek).

De novo Aβ generation assays

For de novo Aβ generation from FPLC fractions, FPLC fractions from culture cell and human brain microsome lysates were incubated for 12 h under nutation with or without spike-in of inhibitors or modulators. Incubated fractions were then concentrated through lyophilizing and reconstituted into 0.05% Triton X-100. Different Aβ isoforms were measured from the resulting samples by ELISA. For de novo Aβ generation from IP samples, immunoprecipitated Sepharose beads from FPLC fractions were incubated in a reaction buffer (50 mM Hepes buffer, 150 mM NaCl, with 0.25% CHAPSO, pH 7.4) at 37°C for 12 h, and different Aβ isoforms were measured from the resulting samples by ELISA.

ELISA

Conditioned culture medium, cell lysates, or in vitro reaction samples were diluted with 1% BSA in wash buffer (TBS supplemented with 0.05% Tween). For the homemade MSD electrochemiluminescent platform, each well of an uncoated 96-well multi-array plate (L15XA-3; Meso Scale Discovery) was coated with 30 µl of a PBS solution containing capture antibody (3 µg/ml 266 for all Aβ ELISAs) and incubated at room temperature overnight, followed by blocking with 5% BSA in wash buffer for 1 h at room temperature with shaking at >300 rpm. A detection antibody solution was prepared with biotinylated detection antibody, 100 ng/ml Streptavidin Sulfo-TAG (R32AD-5; Meso Scale Discovery), and 1% BSA diluted in wash buffer. Following the blocking step, 50 µl/well of the sample, followed by 25 µl/well of detection antibody solution, was incubated for 2 h at room temperature with shaking at >300 rpm, washing wells with wash buffer between incubations. The plate was read and analyzed according to manufacturer protocol. The antibodies used to detect specific antigens were, for Aβ (1–37 specific), D2A6H (rabbit, CST); for Aβ (1–38 specific), 67B8 (mouse, SYSY, RRID: AB_11043334); for Aβ (1–40 specific), HJ-2 (mouse, homemade); for Aβ (1–42 specific), 21F12 (mouse, homemade); for Aβ (1–43 specific), 18584 (rabbit, RRID: AB_2341377; IBL). For the commercial ELISA assay, ELISA for APP-CTFβ, 27776 (IBL); for sAPPβ-sw, K151BUE (Meso Scale Discovery); and for BACE1, DY931 (R&D Systems) were used, and all procedures were done according to manufacturer protocol.

Immunocytochemistry

HEK293 cells were cultured on poly-D-lysine–coated glass-bottom dishes (#1.5 high-tolerance coverglass, 170 ± 5 µm), fixed in 4% PFA in PBS for 15 min, permeabilized by 0.3% Triton X-100 in PBS (PBST), and blocked with 5% skim milk in PBST. For conventional confocal microscope images, after labeling using validated primary antibodies against PS1 N terminus and BACE1 C terminus, cells were washed extensively and incubated with a pair of fluorescence labeled secondary antibodies with Alexa Fluor 488 and 568, and images were acquired with PBS as imaging medium under a 63×, NA 1.4 oil objective using a Carl-Zeiss LSM710 confocal microscope (acquisition software Zen). DAPI was used as counterstain for nuclei. For STED imaging, after labeling using validated primary antibodies against PS1 (E3L9X, rabbit, CST) and BACE1 (MAB9311, mouse, RRID: AB_2061368; R&D Systems), cells were washed extensively and incubated with a pair of fluorescence-labeled secondary antibodies. After staining, cells were treated with a serial mounting medium exchange graded from 10% 2,2′-thiodiethanol (TDE) to 25%, to 50%, and finally to 97%, with each step being a 30-min incubation at room temperature. Images were acquired with 97% TDE as imaging medium using a Leica TCS SP8 STED nanoscope (acquisition software Leica Application Suite X).

PLA

HEK293 cells were fixed in 4% PFA in 0.1 M phosphate buffer for 15 min, permeabilized by 0.3% Triton X-100 in PBS, and blocked with PLA blocking reagent for 30 min at 37°C. After labeling using validated primary antibodies to PS1 N terminus PRB-354P (rabbit, RRID: AB_389690; BioLegend) and BACE1 C terminus MAB5308 (mouse, RRID: AB_95207; Millipore) or TfR 612124 (mouse, RRID: AB_399495; BD Biosciences) as the negative control, cells were washed extensively and incubated with a pair of nucleotide-conjugated secondary antibodies (rabbit PLA

probe Minus and mouse PLA probe Plus) in PLA antibody diluent. Both Minus and Plus PLA probes interact with a rolling-circle nucleotide template when the distance between them is <40 nm. These complexes were ligated in the presence of a ligase in the hybridization solution. The circular template was then amplified using a polymerase, while red-labeled (λ_{ex} 594 nm; λ_{em} 624 nm) probes hybridized the amplified sequence, according to the manufacturer's instructions. In situ PLA images were acquired with PBS as imaging medium under a 63×, NA 1.4 oil objective using a Carl-Zeiss LSM710 confocal microscope (acquisition software Zen). DAPI was used as counterstain for nuclei. Quantification was done by ImageJ (National Institutes of Health; particle analyzer) from five frames of photos containing in total 119 cells for PS1/BACE1 and 106 cells for PS1/TfR.

STED nanoscopy

For STED, cells were imaged with a 100×, NA 1.4 oil objective on a Leica TCS SP8 gated STED nanoscope. Alexa Fluor 488–labeled probes were excited with the 488-nm wavelength of a continuous wave white light (WL) laser (80 MHz) and depleted with a CW 592 nm STED laser with a typical maximum power of 260–300 mW at the back aperture of the objective (corresponding to ∼150 MW/cm^2 in the focal plane), while Alexa Fluor 568–labeled probes were excited with the 568-nm wavelength of a WL laser and depleted with a CW 660-nm STED laser with a typical maximum power of 240–280 mW. All images were acquired in 2D STED mode, i.e., with only lateral resolution improvement. Structures were imaged at settings optimized for a maximum gain in lateral resolution. This corresponded to full depletion laser on an internal Leica GaAsP HyD hybrid detector with a time gate of $2 \le t_g \le 6$ ns for 510–572 nm and $1.63 \le t_g \le 5.13$ ns for 584–626 nm. The resolution at this setting is ∼30 nm (14 nm per pixel). Brightness and contrast of images were adjusted with ImageJ.

Quantification and statistical analysis

All immunocytochemical images were analyzed using ImageJ (National Institutes of Health) software. All statistical analysis was performed using GraphPad Prism 7 software. Statistical details of particular experiments are described in the text and figure legends. Unpaired Student's *t* test was used for all statistical testing. Data distribution was assumed to be normal, but this was not formally tested.

Online supplemental material

Fig. S1 shows the specificity and stability of the β/γ-secretase complex. Fig. S2 shows the distribution of several intramembrane proteases in FPLC fractions of mouse brain and validation of the APP-CTFη expression. Fig. S3 shows the distribution of BACE1 and APP-CTFβ in FPLC fractions of HEK293-swAPP cells and the quantification of mature APP signals in FPLC fractions of HEK293-swAPP cells after treatment with AZD3293 or DMSO as the vehicle control. Fig. S4 shows the successful immunoisolation of HMW β/γ-secretase complexes from FPLC fractions. Fig. S5 shows that a specific TMD is not essential for BACE1 to form the β/γ-secretase complex and generate Aβ.

Acknowledgments

We thank Z. Wang and M. Liao for providing mouse brain and iN cells and M. Ocaña for assistance with STED imaging. We are grateful to members of the Selkoe laboratory for helpful discussions.

This work was funded by National Institutes of Health grants R01 AG06173 (D.J. Selkoe) and P01 AG015379 (M.S. Wolfe and D.J. Selkoe).

D.J. Selkoe is a director of and consultant to Prothena Biosciences. The other authors declare no competing financial interests.

Author contributions: L. Liu, L. Ding, and M. Rovere conducted the experiments; L. Liu, M.S. Wolfe, and D.J. Selkoe designed the experiments, performed data analysis and interpretation, and wrote the paper.

Submitted: 5 July 2018
Revised: 12 October 2018
Accepted: 26 November 2018

References

Bai, X.C., E. Rajendra, G. Yang, Y. Shi, and S.H.W. Scheres. 2015a. Sampling the conformational space of the catalytic subunit of human γ-secretase. *eLife.* 4:1–19. https://doi.org/10.7554/eLife.11182

Bai, X.C., C. Yan, G. Yang, P. Lu, D. Ma, L. Sun, R. Zhou, S.H.W. Scheres, and Y. Shi. 2015b. An atomic structure of human γ-secretase. *Nature.* 525:212–217. https://doi.org/10.1038/nature14892

Baranger, K., M. Khrestchatisky, and S. Rivera. 2016. MT5-MMP, just a new APP processing proteinase in Alzheimer's disease? *J. Neuroinflammation.* 13:167. https://doi.org/10.1186/s12974-016-0633-4

Bolduc, D.M., D.R. Montagna, Y. Gu, D.J. Selkoe, and M.S. Wolfe. 2016a. Nicastrin functions to sterically hinder γ-secretase-substrate interactions driven by substrate transmembrane domain. *Proc. Natl. Acad. Sci. USA.* 113:E509–E518. https://doi.org/10.1073/pnas.1512952113

Bolduc, D.M., D.R. Montagna, M.C. Seghers, M.S. Wolfe, and D.J. Selkoe. 2016b. The amyloid-beta forming tripeptide cleavage mechanism of γ-secretase. *eLife.* 5:1–21. https://doi.org/10.7554/eLife.17578

Brown, M.S., J. Ye, R.B. Rawson, and J.L. Goldstein. 2000. Regulated intramembrane proteolysis: a control mechanism conserved from bacteria to humans. *Cell.* 100:391–398. https://doi.org/10.1016/S0092-8674(00)80675-3

Cacquevel, M., L. Aeschbach, P. Osenkowski, D. Li, W. Ye, M.S. Wolfe, H. Li, D.J. Selkoe, and P.C. Fraering. 2008. Rapid purification of active γ-secretase, an intramembrane protease implicated in Alzheimer's disease. *J. Neurochem.* 104:210–220. https://doi.org/10.1111/j.1471-4159.2007.05041.x

Chasseigneaux, S., and B. Allinquant. 2012. Functions of Aβ, sAPPα and sAPPβ: similarities and differences. *J. Neurochem.* 120(Suppl 1):99–108. https://doi.org/10.1111/j.1471-4159.2011.07584.x

Chen, A.C., L.Y. Guo, B.L. Ostaszewski, D.J. Selkoe, and M.J. LaVoie. 2010. Aph-1 associates directly with full-length and C-terminal fragments of γ-secretase substrates. *J. Biol. Chem.* 285:11378–11391. https://doi.org/10.1074/jbc.M109.088815

Chen, A.C., S. Kim, N. Shepardson, S. Patel, S. Hong, and D.J. Selkoe. 2015. Physical and functional interaction between the α- and γ-secretases: A new model of regulated intramembrane proteolysis. *J. Cell Biol.* 211:1157–1176. https://doi.org/10.1083/jcb.201502001

Chen, F., H. Hasegawa, G. Schmitt-Ulms, T. Kawarai, C. Bohm, T. Katayama, Y. Gu, N. Sanjo, M. Glista, E. Rogaeva, et al. 2006. TMP21 is a presenilin complex component that modulates γ-secretase but not ε-secretase activity. *Nature.* 440:1208–1212. https://doi.org/10.1038/nature04667

Citron, M., D. Westaway, W. Xia, G. Carlson, T. Diehl, G. Levesque, K. Johnson-Wood, M. Lee, P. Seubert, A. Davis, et al. 1997. Mutant presenilins of Alzheimer's disease increase production of 42-residue amyloid β-protein in both transfected cells and transgenic mice. *Nat. Med.* 3:67–72. https://doi.org/10.1038/nm0197-67

Citron, M., C.B. Eckman, T.S. Diehl, C. Corcoran, B.L. Ostaszewski, W. Xia, G. Levesque, P. St George Hyslop, S.G. Younkin, and D.J. Selkoe. 1998. Additive effects of PS1 and APP mutations on secretion of the 42-residue

amyloid β-protein. *Neurobiol. Dis.* 5:107–116. https://doi.org/10.1006/nbdi.1998.0183
Crump, C.J., D.S. Johnson, and Y.M. Li. 2013. Development and mechanism of γ-secretase modulators for Alzheimer's disease. *Biochemistry.* 52:3197–3216. https://doi.org/10.1021/bi400377p
Cui, J., X. Wang, X. Li, X. Wang, C. Zhang, W. Li, Y. Zhang, H. Gu, X. Xie, F. Nan, et al. 2015. Targeting the γ-/β-secretase interaction reduces β-amyloid generation and ameliorates Alzheimer's disease-related pathogenesis. *Cell Discov.* 1:15021. https://doi.org/10.1038/celldisc.2015.21
Edbauer, D., E. Winkler, J.T. Regula, B. Pesold, H. Steiner, and C. Haass. 2003. Reconstitution of γ-secretase activity. *Nat. Cell Biol.* 5:486–488. https://doi.org/10.1038/ncb960
Ermolieff, J., J.A. Loy, G. Koelsch, and J. Tang. 2000. Proteolytic activation of recombinant pro-memapsin 2 (pro-β-secretase) studied with new fluorogenic substrates. *Biochemistry.* 39:12450–12456. https://doi.org/10.1021/bi001494f
Esler, W.P., W.T. Kimberly, B.L. Ostaszewski, W. Ye, T.S. Diehl, D.J. Selkoe, and M.S. Wolfe. 2002. Activity-dependent isolation of the presenilin-γ-secretase complex reveals nicastrin and a γ substrate. *Proc. Natl. Acad. Sci. USA.* 99:2720–2725. https://doi.org/10.1073/pnas.052436599
Farmery, M.R., L.O. Tjernberg, S.E. Pursglove, A. Bergman, B. Winblad, and J. Näslund. 2003. Partial purification and characterization of γ-secretase from post-mortem human brain. *J. Biol. Chem.* 278:24277–24284. https://doi.org/10.1074/jbc.M211992200
Fraering, P.C., M.J. LaVoie, W. Ye, B.L. Ostaszewski, W.T. Kimberly, D.J. Selkoe, and M.S. Wolfe. 2004a. Detergent-dependent dissociation of active γ-secretase reveals an interaction between Pen-2 and PS1-NTF and offers a model for subunit organization within the complex. *Biochemistry.* 43:323–333. https://doi.org/10.1021/bi035748j
Fraering, P.C., W. Ye, J.M. Strub, G. Dolios, M.J. LaVoie, B.L. Ostaszewski, A. van Dorsselaer, R. Wang, D.J. Selkoe, and M.S. Wolfe. 2004b. Purification and characterization of the human γ-secretase complex. *Biochemistry.* 43:9774–9789. https://doi.org/10.1021/bi0494976
Gu, Y., N. Sanjo, F. Chen, H. Hasegawa, A. Petit, X. Ruan, W. Li, C. Shier, T. Kawarai, G. Schmitt-Ulms, et al. 2004. The presenilin proteins are components of multiple membrane-bound complexes that have different biological activities. *J. Biol. Chem.* 279:31329–31336. https://doi.org/10.1074/jbc.M401548200
Haapasalo, A., and D.M. Kovacs. 2011. The many substrates of presenilin/γ-secretase. *J. Alzheimers Dis.* 25:3–28. https://doi.org/10.3233/JAD-2011-101065
Haass, C., M.G. Schlossmacher, A.Y. Hung, C. Vigo-Pelfrey, A. Mellon, B.L. Ostaszewski, I. Lieberburg, E.H. Koo, D. Schenk, D.B. Teplow, et al. 1992. Amyloid β-peptide is produced by cultured cells during normal metabolism. *Nature.* 359:322–325. https://doi.org/10.1038/359322a0
Jumpertz, T., A. Rennhack, J. Ness, S. Baches, C.U. Pietrzik, B. Bulic, and S. Weggen. 2012. Presenilin is the molecular target of acidic γ-secretase modulators in living cells. *PLoS One.* 7:e30484. https://doi.org/10.1371/journal.pone.0030484
Kimberly, W.T., M.J. LaVoie, B.L. Ostaszewski, W. Ye, M.S. Wolfe, and D.J. Selkoe. 2003. γ-secretase is a membrane protein complex comprised of presenilin, nicastrin, Aph-1, and Pen-2. *Proc. Natl. Acad. Sci. USA.* 100:6382–6387. https://doi.org/10.1073/pnas.1037392100
Kornilova, A.Y., F. Bihel, C. Das, and M.S. Wolfe. 2005. The initial substrate-binding site of γ-secretase is located on presenilin near the active site. *Proc. Natl. Acad. Sci. USA.* 102:3230–3235. https://doi.org/10.1073/pnas.0407640102
Li, Y.-M., M.-T. Lai, M. Xu, Q. Huang, J. DiMuzio-Mower, M.K. Sardana, X.-P. Shi, K.-C. Yin, J.A. Shafer, and S.J. Gardell. 2000a. Presenilin 1 is linked with γ-secretase activity in the detergent solubilized state. *Proc. Natl. Acad. Sci. USA.* 97:6138–6143. https://doi.org/10.1073/pnas.110126897
Li, Y.M., M. Xu, M.T. Lai, Q. Huang, J.L. Castro, J. DiMuzio-Mower, T. Harrison, C. Lellis, A. Nadin, J.G. Neduvelil, et al. 2000b. Photoactivated γ-secretase inhibitors directed to the active site covalently label presenilin 1. *Nature.* 405:689–694. https://doi.org/10.1038/35015085
Li, Y., S.H.J. Lu, C.J. Tsai, C. Bohm, S. Qamar, R.B. Dodd, W. Meadows, A. Jeon, A. McLeod, F. Chen, et al. 2014. Structural interactions between inhibitor and substrate docking sites give insight into mechanisms of human PS1 complexes. *Structure.* 22:125–135. https://doi.org/10.1016/j.str.2013.09.018
Martin, L., R. Fluhrer, K. Reiss, E. Kremmer, P. Saftig, and C. Haass. 2008. Regulated intramembrane proteolysis of Bri2 (Itm2b) by ADAM10 and SPPL2a/SPPL2b. *J. Biol. Chem.* 283:1644–1652. https://doi.org/10.1074/jbc.M706661200
Muratore, C.R., C. Zhou, M. Liao, M.A. Fernandez, W.M. Taylor, V.N. Lagomarsino, R.V. Pearse II, H.C. Rice, J.M. Negri, A. He, et al. 2017. Cell-type Dependent Alzheimer's Disease Phenotypes: Probing the Biology of Selective Neuronal Vulnerability. *Stem Cell Reports.* 9:1868–1884. https://doi.org/10.1016/j.stemcr.2017.10.015
Ran, F.A., P.D. Hsu, J. Wright, V. Agarwala, D.A. Scott, and F. Zhang. 2013. Genome engineering using the CRISPR-Cas9 system. *Nat. Protoc.* 8:2281–2308. https://doi.org/10.1038/nprot.2013.143
Rawson, R.B., N.G. Zelenski, D. Nijhawan, J. Ye, J. Sakai, M.T. Hasan, T.Y. Chang, M.S. Brown, and J.L. Goldstein. 1997. Complementation cloning of S2P, a gene encoding a putative metalloprotease required for intramembrane cleavage of SREBPs. *Mol. Cell.* 1:47–57. https://doi.org/10.1016/S1097-2765(00)80006-4
Reinhard, C., S.S. Hébert, and B. De Strooper. 2005. The amyloid-β precursor protein: integrating structure with biological function. *EMBO J.* 24:3996–4006. https://doi.org/10.1038/sj.emboj.7600860
Sato, C., Y. Morohashi, T. Tomita, and T. Iwatsubo. 2006. Structure of the catalytic pore of γ-secretase probed by the accessibility of substituted cysteines. *J. Neurosci.* 26:12081–12088. https://doi.org/10.1523/JNEUROSCI.3614-06.2006
Selkoe, D.J., and J. Hardy. 2016. The amyloid hypothesis of Alzheimer's disease at 25 years. *EMBO Mol. Med.* 8:595–608. https://doi.org/10.15252/emmm.201606210
Seubert, P., C. Vigo-Pelfrey, F. Esch, M. Lee, H. Dovey, D. Davis, S. Sinha, M. Schlossmacher, J. Whaley, C. Swindlehurst, et al. 1992. Isolation and quantification of soluble Alzheimer's β-peptide from biological fluids. *Nature.* 359:325–327. https://doi.org/10.1038/359325a0
Shoji, M., T.E. Golde, J. Ghiso, T.T. Cheung, S. Estus, L.M. Shaffer, X.D. Cai, D.M. McKay, R. Tintner, B. Frangione, et al. 1992. Production of the Alzheimer amyloid beta protein by normal proteolytic processing. *Science.* 258:126–129. https://doi.org/10.1126/science.1439760
Sun, L., L. Zhao, G. Yang, C. Yan, R. Zhou, X. Zhou, T. Xie, Y. Zhao, S. Wu, X. Li, and Y. Shi. 2015. Structural basis of human γ-secretase assembly. *Proc. Natl. Acad. Sci. USA.* 112:6003–6008. https://doi.org/10.1073/pnas.1506242112
Takasugi, N., T. Tomita, I. Hayashi, M. Tsuruoka, M. Niimura, Y. Takahashi, G. Thinakaran, and T. Iwatsubo. 2003. The role of presenilin cofactors in the γ-secretase complex. *Nature.* 422:438–441. https://doi.org/10.1038/nature01506
Tian, Y., J.C. Chang, E.Y. Fan, M. Flajolet, and P. Greengard. 2013. Adaptor complex AP2/PICALM, through interaction with LC3, targets Alzheimer's APP-CTF for terminal degradation via autophagy. *Proc. Natl. Acad. Sci. USA.* 110:17071–17076. https://doi.org/10.1073/pnas.1315110110
Tomita, S., Y. Kirino, and T. Suzuki. 1998. Cleavage of Alzheimer's amyloid precursor protein (APP) by secretases occurs after O-glycosylation of APP in the protein secretory pathway. Identification of intracellular compartments in which APP cleavage occurs without using toxic agents that interfere with protein metabolism. *J. Biol. Chem.* 273:6277–6284. https://doi.org/10.1074/jbc.273.11.6277
Vassar, R., P.H. Kuhn, C. Haass, M.E. Kennedy, L. Rajendran, P.C. Wong, and S.F. Lichtenthaler. 2014. Function, therapeutic potential and cell biology of BACE proteases: current status and future prospects. *J. Neurochem.* 130:4–28. https://doi.org/10.1111/jnc.12715
Wakabayashi, T., K. Craessaerts, L. Bammens, M. Bentahir, F. Borgions, P. Herdewijn, A. Staes, E. Timmerman, J. Vandekerckhove, E. Rubinstein, et al. 2009. Analysis of the γ-secretase interactome and validation of its association with tetraspanin-enriched microdomains. *Nat. Cell Biol.* 11:1340–1346. https://doi.org/10.1038/ncb1978
Willem, M., S. Tahirovic, M.A. Busche, S.V. Ovsepian, M. Chafai, S. Kootar, D. Hornburg, L.D.B. Evans, S. Moore, A. Daria, et al. 2015. η-Secretase processing of APP inhibits neuronal activity in the hippocampus. *Nature.* 526:443–447. https://doi.org/10.1038/nature14864
Wolfe, M.S., W. Xia, B.L. Ostaszewski, T.S. Diehl, W.T. Kimberly, and D.J. Selkoe. 1999. Two transmembrane aspartates in presenilin-1 required for presenilin endoproteolysis and γ-secretase activity. *Nature.* 398:513–517. https://doi.org/10.1038/19077